NAVAL POSTGRADUATE SCHOOL
Monterey, California

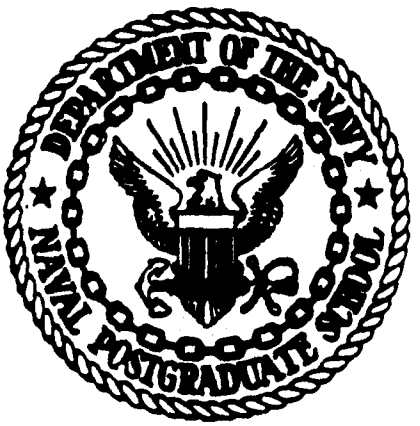

THESIS

AERODYNAMIC STABILIZATION OF AN
ELECTRICAL DISCHARGE FOR GAS LASERS

by

Charles Herbert Davis

September 1980

Thesis Advisor: O. Biblarz

Approved for public release; distribution unlimited

SECURITY CLASSIFICATION OF THIS PAGE (When Data Entered)

REPORT DOCUMENTATION PAGE

READ INSTRUCTIONS BEFORE COMPLETING FORM

1. REPORT NUMBER	2. GOVT ACCESSION NO. AD-A093 020
3. RECIPIENT'S CATALOG NUMBER	
4. TITLE (and Subtitle) (6) Aerodynamic Stabilization of an Electrical Discharge for Gas Lasers.	5. TYPE OF REPORT & PERIOD COVERED (9) Master's Thesis; (September 1980)
	6. PERFORMING ORG. REPORT NUMBER
7. AUTHOR(s) (10) Charles Herbert Davis	8. CONTRACT OR GRANT NUMBER(s) (12) 105
9. PERFORMING ORGANIZATION NAME AND ADDRESS Naval Postgraduate School Monterey, California 93940	10. PROGRAM ELEMENT, PROJECT, TASK AREA & WORK UNIT NUMBERS
11. CONTROLLING OFFICE NAME AND ADDRESS (11) Naval Postgraduate School Monterey, California 93940	12. REPORT DATE September 1980
	13. NUMBER OF PAGES 104
14. MONITORING AGENCY NAME & ADDRESS(if different from Controlling Office) Naval Postgraudate School Monterey, California 93940	15. SECURITY CLASS. (of this report) Unclassified
	15a. DECLASSIFICATION/DOWNGRADING SCHEDULE

16. DISTRIBUTION STATEMENT (of this Report)

Approved for public release; distribution unlimited

17. DISTRIBUTION STATEMENT (of the abstract entered in Block 20, if different from Report)

18. SUPPLEMENTARY NOTES

19. KEY WORDS (Continue on reverse side if necessary and identify by block number)

Electrical lasers, discharge stabilization, turbulence production

20. ABSTRACT (Continue on reverse side if necessary and identify by block number)

This work reports on a study of a subsonic, turbulent, diffuse discharge with potential application to electric discharge convection lasers. Two methods of turbulence generation have been investigated, namely, a pulsed-jet ejector and a plate generator. Power inputs for various flow conditions are reported. Turbulence spectra for these flow conditions have been studied and an effort made to optimize the discharge stabilizing properties of the flow. Plate generated turbulence proved superior for stabilizing the discharge.

DD FORM 1 JAN 73 1473 EDITION OF 1 NOV 65 IS OBSOLETE
S/N 0102-014-6601

(Page 1)

132450

SECURITY CLASSIFICATION OF THIS PAGE (When Data Entered)

Approved for Public Release, Distribution Unlimited

Aerodynamic Stabilization of an Electrical Discharge for Gas Lasers

by

Charles Herbert Davis
Lieutenant, United States Coast Guard
B.A, Wittenberg University, 1970

Submitted in partial fulfillment of the
requirements for the degrees of

MASTER OF SCIENCE IN AERONAUTICAL ENGINEERING
and
MASTER OF SCIENCE IN ELECTRICAL ENGINEERING

from the

NAVAL POSTGRADUATE SCHOOL
September 1980

Author _____

Approved by:

_____
Thesis Advisor

_____
Co-Advisor

_____
Chairman, Department of
Aeronautical Engineering

_____
Chairman, Department of
Electrical Engineering

_____
Dean of Science and Engineering

ABSTRACT

This work reports on a study of a subsonic, turbulent, diffuse discharge with potential application to electric discharge convection lasers. Two methods of turbulence generation have been investigated; namely, a pulsed-jet ejector and a plate generator. Power inputs for various flow conditions are reported. Turbulence spectra for these flow conditions have been studied and an effort made to optimize the discharge stabilizing properties of the flow. Plate generated turbulence proved superior for stabilizing the discharge.

TABLE OF CONTENTS

LIST OF FIGURES

ACKNOWLEDGEMENTS

Many people made an important contribution in bringing this work to fruition. Thank you Dr. Ray Dacey and Dr. B. G. Schumacher of the University of Oklahoma, for the original inspiration. For the assistance in course scheduling and giving me the opportunity, Prof. R. D. Strum and Prof. Robert Zucker. For the additional work effort in coordinating my double degree program, Prof. D. E. Kirk and Prof. M. F. Platzer. A special accolade to Bob Besel and Ted Dunton and their staffs for the technical support in remodeling and repair of the experimental apparatus.

I deeply appreciate the almost daily tutoring of LCDR J. L. Barto on the subject matter as well as his assistance in the laboratory. For their daily guidance and support, I am indebted to my thesis advisors, Prof. Oscar Biblarz and Prof. John Powers. But the person, to whom I owe the most, is my wife. I love you, Nancy.

I. INTRODUCTION

The purpose of this research was to investigate aerodynamic methods of stabilizing the electric discharge in the cavity of gas lasers. Primarily, turbulence was studied as a means to stabilize the discharge; turbulence permits more power to be coupled into the cavity. No attempt was made in this work to actually lase the medium.

From previous investigations, higher power inputs are thought to be associated with turbulence spectra that are more intense at lower frequencies [Refs. 11, 17, 30, 34]. To investigate the way turbulence affects the discharge, two sets of tests have been performed. Current and voltages have been measured to determine the amount of power that can be coupled into the cavity under various flow conditions. The other test involved measuring the velocities and turbulence spectra in the cavity, i.e., those flow conditions that were associated with certain power inputs. The total effort here was directed at optimizing the flow parameters in order to achieve a maximum power into the cavity with a minimum work input.

A. DISCUSSION OF THESIS FORMAT

This paper is divided into seven sections. In Sec. I, a review is presented on the principles of laser operation

and aerodynamic discharge stabilization. First, the theory and operation of the CO_2 electrical laser is described. The NASA Lewis convection laser is detailed as an example of the application of this technology. The final part of the introduction demonstrates how the mechanisms of convection and turbulence may be used to stabilize the electric discharge. The reader who is familiar with these topics may wish to proceed directly to Sec. II. Section II discusses the evolution of the system used at the Naval Postgraduate School for investigating discharge stability. The system presently being used is an extension of the design used in past studies at this institution. The experimental apparatus including the flow systems, discharge circuit and diagnostic equipment is presented in Sec. III. Basically, two sets of tests were performed on the discharge as shown in Sec. IV. One test involved measuring the turbulence frequency and intensity in the cavity; the other test measured the power coupled into the discharge under various conditions.

The results of both tests are discussed in Sec. V. A critical experimental parameter is arrived at from the fact that turbulence became less effective at short gaps and higher flow rates as shown in the data. In Sec. VI., it is concluded that high frequency, low intensity turbulence has a stabilizing effect on the discharge and that this low frequency turbulence can be generated through the pulsed-jet

ejector principle. Finally, some recommendations for future work are made in Sec. VII.

B. DEVELOPMENT OF THE CO_2 LASER

In 1963, Mathias and Parker were the first to discover the molecular laser. They observed oscillations on a number of lines in nitrogen using high current short duration discharges [Ref. 1]. Patel successfully predicted the enhancement of Co_2 laser action at 10.6 μm using N_2 for pumping [Ref. 2]. The carbon dioxide laser realization soon followed and was recognized as an efficient source of high power [Ref. 3].

In the CO_2 electrical laser, an understanding of the way energy is stored is requisite to an understanding of the operation of the laser itself. The integral energy of the CO_2 molecule is stored in three electronic states -- rotation, vibration and translation. The rotation energy is small and can usually be neglected. All these energy forms can be assigned a specific value representing a particular level of energy. Furthermore, the number of molecules excited to a particular energy level can be predicted accurately at equilibrium by Boltzmann statistics.

Every molecule has a characteristic vibrational temperature $\theta_v = \frac{h\nu}{k}$. Boltzmann predicts the population of an energy level, n_v:

$$\frac{n_v}{n} = \left\{ \exp\left(- \frac{V\theta_r}{T} \right) \right\} \left\{ 1 - \exp\left(- \frac{\theta_v}{T} \right) \right\} , \qquad (1)$$

where v is the vibrational quantum number and T is the absolute temperature of the gas [Ref. 4]. This close relationship between the intermolecular vibrational energy transfer and the absolute temperature of a gas observed in the above equation arises because of the speed, efficiency, and resonance character of the vibrational energy transfer. Using the Boltzmann equation, the energy distribution is characterized by vibrational temperatures [Ref. 8]. The statistics are more complicated for the CO_2 molecule because degenerate states exist.

A state of molecule is a condition defined by a set of quantum numbers. LEVEL refers to energy values associated with different states. Different STATES may have the same ENERGY level [Ref. 4], in which case the state is degenerate. The degeneracy is an integer number equal to the number of states with the same energy.

For CO_2, four linear modes of vibration are observed (Fig 1): Symmetric stretch, asymmetric stretch, and two degenerate bending modes of equal energy [Ref. 5]. Because CO_2 is a linear molecule and only one degeneracy is excited, exact quantum numbers can be defined [Ref. 6]. For CO_2, four vibrational quantum numbers are needed to find the equilibrium population and energy: m is the quantum number for the symmetric stretch or ν_1

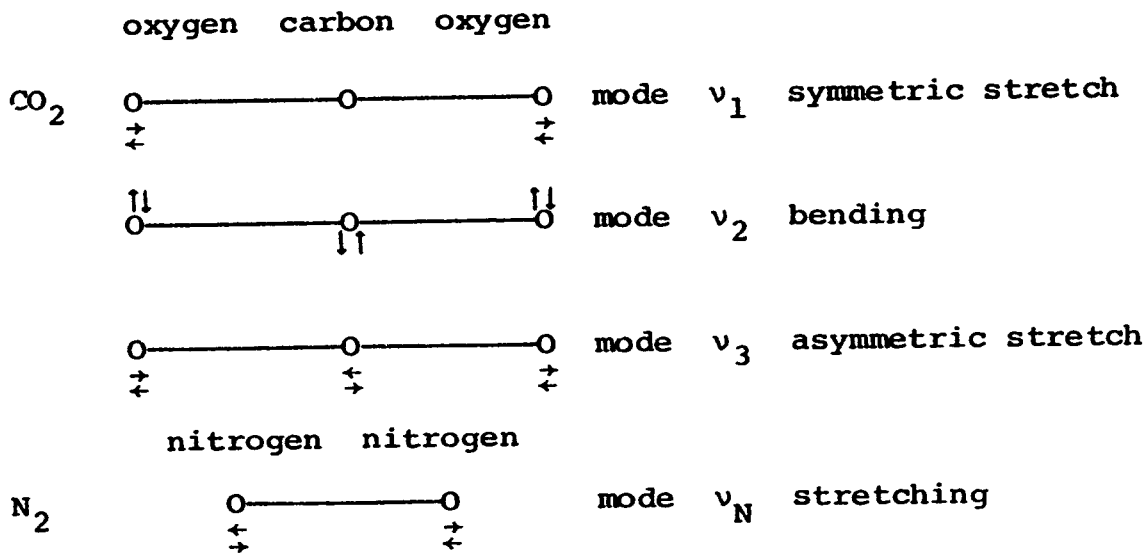

Vibrational Modes for CO_2-N_2

Figure 1

mode, q for the asymmetric stretch or ν_3 mode, and n and p are for the bending mode ν_2. The equation for the calculation of population in CO_2 is [Ref. 4]

$$\frac{n(m,r,q)}{n} = \left\{\exp\left(-\frac{m\theta_1}{T}\right)\right\}\left\{1-\exp\left(-\frac{\theta_1}{T}\right)\right\} \times$$

$$\left\{(r+1)\exp\left(-\frac{r\theta_2}{T}\right)\right\}\left\{1-\exp\left(-\frac{\theta_2}{T}\right)\right\} \times \qquad (2)$$

$$\left\{\exp\left(-\frac{q\theta_3}{T}\right)\right\}\left\{1-\exp\left(-\frac{\theta_3}{T}\right)\right\} \quad .$$

Therefore, each level has a population, which in turn determines an amount of energy associated with this population distribution among levels. Also, the symmetric stretch and bending modes are coupled collisionally by the Fermi resonance between them. This coupling permits the prediction of these modal energy distributions by single vibrational temperature [Ref. 8].

One important criterion for lasing is the achievement of a population inversion. The population inversion, as the name implies, is present when the number of molecules excited to a higher energy level exceeds the number of molecules in a lower level. By inspecting the gain equation, the importance of the population is apparent [Ref. 7]:

$$\frac{(dI)_\nu}{I_\nu} = (B_{12})_\nu \left(\frac{g_1}{g_2} N_2 - N_1\right) h\nu dx \ , \qquad (3)$$

where N_2 and N_1 are the populations of energy levels ε_2 and ε_1, respectively, g_1 and g_2 account for possible degeneracies, B_{12} is the Einstein coefficient of stimulated absorption, h is Planck's constant and x is the length through the gas. Therefore, for a positive amplification of the intensity I_o, more molecules are required to reside in the higher ε_2 level [Ref. 5].

The small gain coefficient, α_o, is a direct measure of the population inversion. The small signal gain is the fractional change of the intensity of radiation flux through the plasma. The saturation intensity, I_s, is the value of the spectral radiation intensity, I_ν, for which the value of the gain is reduced to $\alpha_o/2$. The maximum optical power density is $\alpha_o I_s$, [Ref. 8]. The small signal gain coefficient, α_o, is the negative of the spectral absorption coefficient α_ν. The spectral absorption describes the changes in intensity through the gas as a function of frequency. If the intensity decreases through the gas, then α_ν is defined as a positive number; if intensity increases, then α_ν is negative [Ref. 5]:

$$(dI)_\nu = \alpha_\nu I_\nu dx \ . \qquad (4)$$

After integrating over the length of the gas and making a substitution for

$$B_{12} = \frac{c^2}{8\pi h\nu^3} A_{21} \,, \tag{5}$$

where A_{21} is Einstein's spontaneous emission coefficient (the transition probability), the spectral absorption coefficient is in general terms [Ref. 5].

$$\alpha_\nu = \frac{c^2}{8\pi\nu^2} (A_{21})_\nu (N_1 - \frac{g_1}{g_2} N_2) \tag{6}$$

The function line shape, $g(\nu)$, has been experimentally found to follow the Lorentzian line shape due to the dominance of collision broadening.

Collision broadening and Doppler broadening contribute to an increase in the bandwidth of the lasing frequency or line shape. Doppler broadening predominates in thermally excited, low density gases. Collision broadening is the spread in lasing frequency due to the collision of a radiating molecule with another. The collision probability is proportional to $P/\sqrt{T}$. Therefore, collision broadening tends to dominate in dense, high pressure and low temperature mediums. Both types of broadening can make a contribution to the bandwidth in the CO_2 laser.

As stated previously, a population inversion must exist in order to have lasing. Therefore, lasers are

non-equilibrium devices. This non-equilibrium is accomplished by pumping or exciting the collection of molecules to an excited state. But the molecules, if undisturbed, will naturally return to their unexcited equilibrium in a predetermined length of time known as the relaxation time, τ. Relaxation processes may involve a combination of three mechanisms: collisions between molecules, spontaneous emission, and interaction between photons and molecules. Elastic collisions between molecules do not change internal degrees of freedom. Conversely, inelastic collisions change the excitation or energy of the internal degrees of freedom: vibration or rotation.

If the collisions were inelastic, the translational kinetic energy may transfer to internal vibration energy; this process is called a V-T reaction. If the vibrational internal energy of one molecule is transferred to vibrational energy of another molecule, the process is called a V-V reaction. The V-V reaction is much faster than the V-T reaction.

Translational relaxation is very rapid and the velocities of molecules on the same scale have been observed to follow the Maxwell distribution. Translational relaxation is proportional to the square root of gas temperature and inversely proportional to the gas pressure. Vibrational relaxation has an exponential dependence on the cube root of temperature and is a slower process. The

difference in the relaxation helps to maintain a vibrationally excited state in the gas once achieved [Ref. 4].

In the diagram, Fig. 2, the vibrational energy levels of the CO_2-N_2 laser are shown. Some of the important vibrational and translational collision energy transfers as well as the radiative processes are shown and numbered. For a CO_2-N_2-H_e laser mixture in equilibrium, the processes are described:

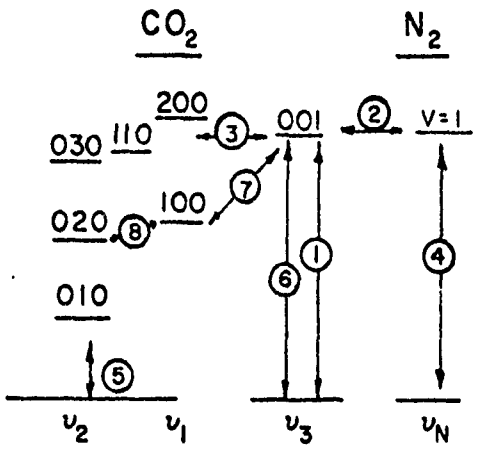

Vibrational Level of CO_2 and N_2 Modes

Figure 2

1. electron excitation and de-excitation (V-T energy exchange) of ν_3,
2. efficient and nearly resonant V-V energy exchange between ν_N and ν_3,

3. non-Maxwellian V-V energy exchange between ν_3 and ν_2 and ν_1.
4. electron excitation and de-excitation (V-T exchange) of $\nu_{N'}$
5. non-Maxwellian excitation and de-excitation (V-T exchange by both electrons and heavy particles of ν_2),
6. Noncoherent absorption and spontaneous emission of radiation of ν_3 at 4.3μm,
7. coherent absorption and stimulated emission of radiation from 001 to 100 of CO_2 at 10.6 μm,
8. non-Maxwellian V-V energy exchange between ν_2 and ν_1 [Ref. 8].

The long metastable state of N_2, which excites ν_3, is important in maintaining the population of 001 of CO_2, the upper lasing level. The laser is more efficient where the transfers that may contribute to losses in the population of 001 are minimized or slowed. These detrimental transfers are processes 1, 3 and 6. Transfers 2, 4, 5 and 8 assist in producing the population inversion. Processes 2 and 4 are instrumental in maintaining the population of the upper laser level, while processes 5 and 8 assist in evacuating 001 of CO_2, the lower laser level. These transfers, as well as the lasing itself, can be controlled through various techniques of stabilization and optimization for maximum laser power.

The maximum laser power or optical power density is given by

$$P_L = \alpha_o I_s \tag{7}$$

and can be related to the electrical power, P_E, given by

$$P_E = E \cdot J \ , \tag{8}$$

where E indicates the electric field and J the current density. The relationship between P_L and P_E is

$$P_L = \eta F P_E \ , \tag{9}$$

where η is the quantum efficiency and F is the fraction of electric power that excites molecules to states that eventually lase. After some substitutions and rearrangement, Eq. (8) can be written

$$P_e = n^2 \left(\frac{E}{n}\right)^2 \frac{n_e}{n} \frac{e^2}{m_e \sigma_e \bar{v}} \tag{10}$$

where n is the number density of ions and electrons, n_e is the number density of electrons, m_e is electron mass, σ_e is electron conductivity and $\bar{v}$ is average electron velocity. This equation emphasizes the importance of three parameters to be controlled in electrical lasers: N^2, E/n, n_e/n. The ratio of E to n defines the electron energy and n_e to

η, the fraction of electrons to lase in the plasma [Ref. 4] Since the number density, n^2, is proportional to pressure squared, a higher pressure implies more power (Fig. 3) [Ref. 8].

Therefore, the same power can be obtained from a smaller cavity at a higher pressure or more power from the same cavity a higher pressure [Ref. 4].

Electron energy increases kinetically as the electron accelerates from the cathode to the anode in the laser cavity. As the electron traverses the cavity, collisions occur and if the collision is inelastic, the electron will give up some of the acquired kinetic energy to increasing its own or some other molecules internal energy. These collisions occur on the average at distances equal to the mean free path, λ. The kinetic energy given is λE. Recalling from the Boltzmann relations that electron energies can be related to characteristic vibrational temperatures, an exact amount of energy is needed to pump or excite a particular state. Therefore, to excite nitrogen's first vibrational level (Fig. 2, process 4) a particular value of E/n is needed. Referring again to Fig. 2, the evacuation of the lower laser level (processes 5 and 8) also defines a particular E/n, the role of helium in the mixture [Ref. 9]. The mixture constituency, molal balance and gas pressure are critical to determining the E/n, but a parameter known as the ionization coefficient, Z, is also

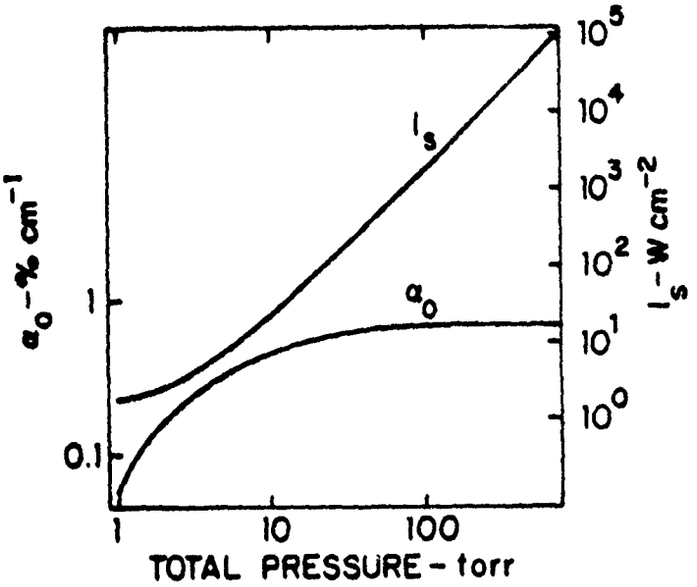

The quantities α_0 and I_s as a function of the total gas pressure for a 10% CO_2, 10% N_2, 80% He gas mixture at 450°K and a reduced average energy of 1.50 eV [Ref. 8].

Figure 3

important [Ref. 9]. The effectiveness of ionization depends on the electron velocity and the electron cross section [Ref. 10]. The ionization coefficient can be defined by a second order, non-linear partial differential equation, assuming axial velocity only in the cavity and radial symmetric diffusion of ions [Ref. 11].

$$U \frac{\partial n}{\partial x} - \frac{1}{r} \left(rD_a \frac{\partial n}{\partial r}\right) = Z_n - \alpha n^3 \tag{11}$$

where D_a is the ambipolar diffusion coefficient and Z the ionization coefficient.

Relatively low values of E/n ($<100 \times 10^{-21}$ Vm^2) are used in high power CO_2-N_2-H_e lasers [Ref. 9]. Limbeck and Lucas show the effects of varying mixtures, pressures and ionization, coefficients, and heating on E/n. Generally higher pressures and more helium are useful in obtaining $E/n \doteq 20 \times 10^{-21}$, which are optimum for CO_2-N_2-H_e lasers. The apparatus used was a sealed or low flow laser (Fig. 4) capable of producing approximately 4W of continuous or 60W pulsed power.

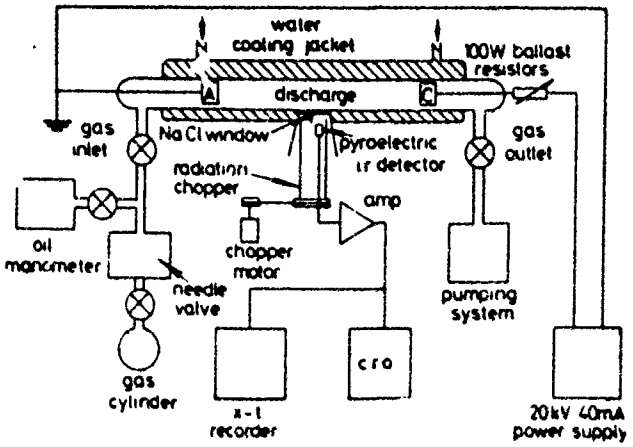

Fig. 4 Sealed or low flow CO_2 laser schematic [Ref. 9]

The major problem with the sealed laser is in providing a reaction path whereby the products of the dissociation of CO_2 can be regenerated to form CO_2 [Ref. 5]. Cooling the medium is also necessary to maintain an optimum E/n.

About 1969, T. F. Deutsch developed a fast axial flow system that used the properties of convection to both cool and remove dissociated products [Ref. 12]. DeMaria [Ref. 13], in 1973, modelled the relationship between laser power and convective cooling through $\alpha_o I_s$. DeMaria showed that

$$\alpha = \frac{\alpha_o}{1 + 2\sigma I \tau_F / h\nu} , \tag{13}$$

$$I_s = \frac{h\nu}{2\sigma\tau_F} \tag{14}$$

where σ is the cross section for stimulated emission, τ_f is the residence time and equals L_c/V_f, L_c is the length of discharge region parallel to gas flow and is called the interelectrode gap or cavity length, and V_f is the gas flow rate. This model confirmed Fowler's observations of rapid decline of power density with increasing gas temperature and constant n_e [Ref. 8], as shown in Fig. 5.

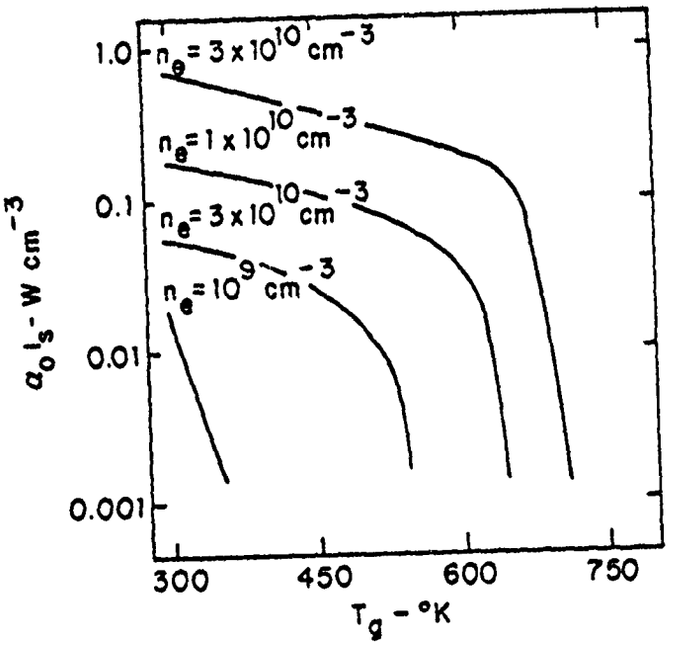

Optical power density $\alpha_o I_s$ as a function of T_g and n_e for a gas mixture of 1 Torr CO_2, 1 Torr N_2, 8 Torr He and a reduced average energy of 1.50 eV. [Ref. 8].

Figure 5

The NASA Lewis Research Center has designed a continuous wave (CW) CO_2 laser capable of delivering up to 70KW of power. This laser is closed cycle (Fig. 6) and uses large adaptive optics [Ref. 14]. A method for improving the peak power out of the laser is to pulse the discharge. In 1970, Tyte reported peak powers 500 times greater than CW from the same system. In 1968, Hill achieved 1-MW peak power with a 20% efficiency at a rate of 30 pps [Ref. 5].

NASA became involved in a program to define and evaluate the potential of high-power lasers. Although interested in primarily shorter wavelength, the CO_2 laser offered a high level of technological maturity. The design criteria, [Ref. 14] were:

(1) Optimum electric excitation method for long-duration, high-power operation

(2) System efficiency

(3) Chemical poisoning effects on gas mixtures

(4) Optimum optical cavity configuration effects for best beam quality.

The approach was to first investigate the performance of electrical excitation and the electron beam sustained discharge. The electrical excitation method was the pin-to-plane, self-sustained, transverse gas transverse discharge system [Ref. 5]. Many methods have been suggested as solutions to the electron avalanche control problem, but these are complicated. Therefore, because of simplicity,

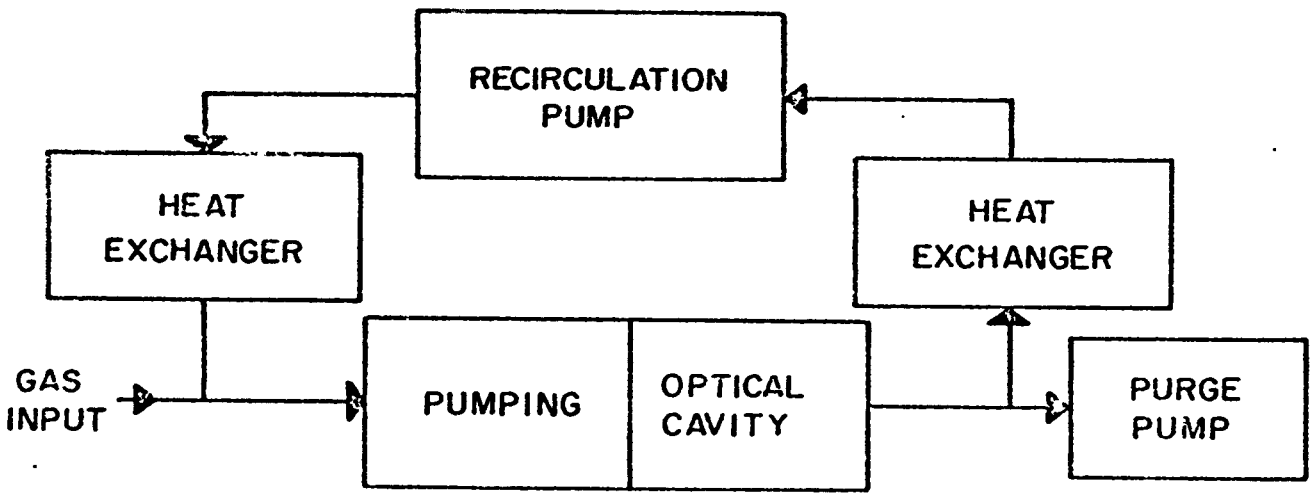

Block Diagram of Closed Cycle
Flowing Gas Laser (Ref. [13j p. 745)

Figure 6

the self-sustained discharge should be investigated further to determine how much stability this system alone may yield [Ref. 14].

Another limitation on the high power lasers has been traditionally the dissociated products of the lasing gases due to lasing itself. NASA intended to study these effects and determine means of overcoming these problems under the supervision of R. B. Lancashire [Ref. 14]. The NASA designed optical cavity accommodated differing beam sizes, paths and discharges [Ref. 14].

The NASA system is, in general, similar to the system described in the block diagram in Fig. 6. The purge pump is much more effective in obtaining a hard vacuum so that contamination of the lasing gas by residuals can be neglected. Also, somewhat unique to the NASA system is the large pressure range operation which demands a recirculating gas pump capable of delivering 100-800 Torr static pressure in the cavity. A hermetical seal obviates using makeup gases and improves system efficiency. The NASA system has only one heat exchanger. Because of the large pressure range, a diffuser was mounted downstream of the cavity to recover 80 percent head [Ref. 14].

The cavity incorporates the flexibility to accommodate the two methods of excitation discussed with only minor modification (Fig. 7). The optical cavity can change its

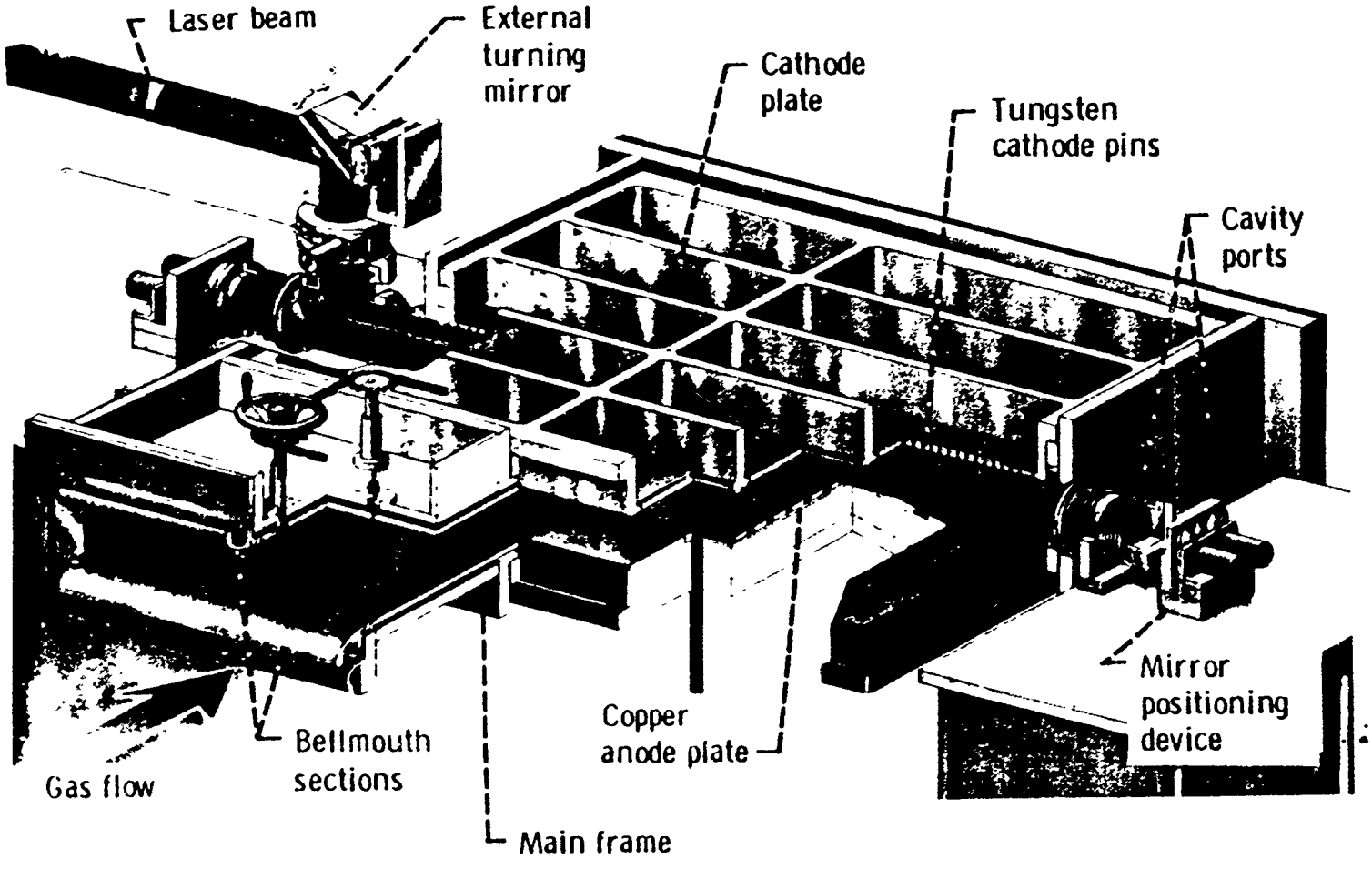

Fig. 7 Lancashire's laser cavity [Ref. 14]

configuration to make a variety of folded unstable resonators or oscillator-amplifier combinations [Ref. 14].

In the pin-to-plane discharge, 16 rows of pins with 5-cm spacing preionize the gas through row 7 and form the discharge in the optical cavity, rows 7-16. The non-symmetric row input power density in the cavity provides a uniform gain path which in turn helps make a uniform output laser beam (Fig. 8). As in the case of the sealed gas laser, the gross gain is still a primary function of n, n_e and E/n (note E/n < 100 x 10^{-21} V-m^2) [Ref. 14].

Lancashire projected that electrical efficiencies greater than 20 percent and power outputs of approximately 20 KW per channel could be achieved with the NASA system. Multichannel outputs would have to be determined experimentally because of nonlinearities of discharge and heating effects. Lancashire discovered that greater than twice the output power could be attained using the electron-beam-sustained discharge with the same efficiency. This higher power results from the greater control of electron source and sustainer field enabling great power inputs with discharge stability. Lancashire concludes, however, that the pin-to-plane discharge may be advantageous because of simplicity and reliability [Ref. 14].

Optical excitation as a means of pumping gas lasers is discussed by C.R. Jones [Ref.15]. This method has only

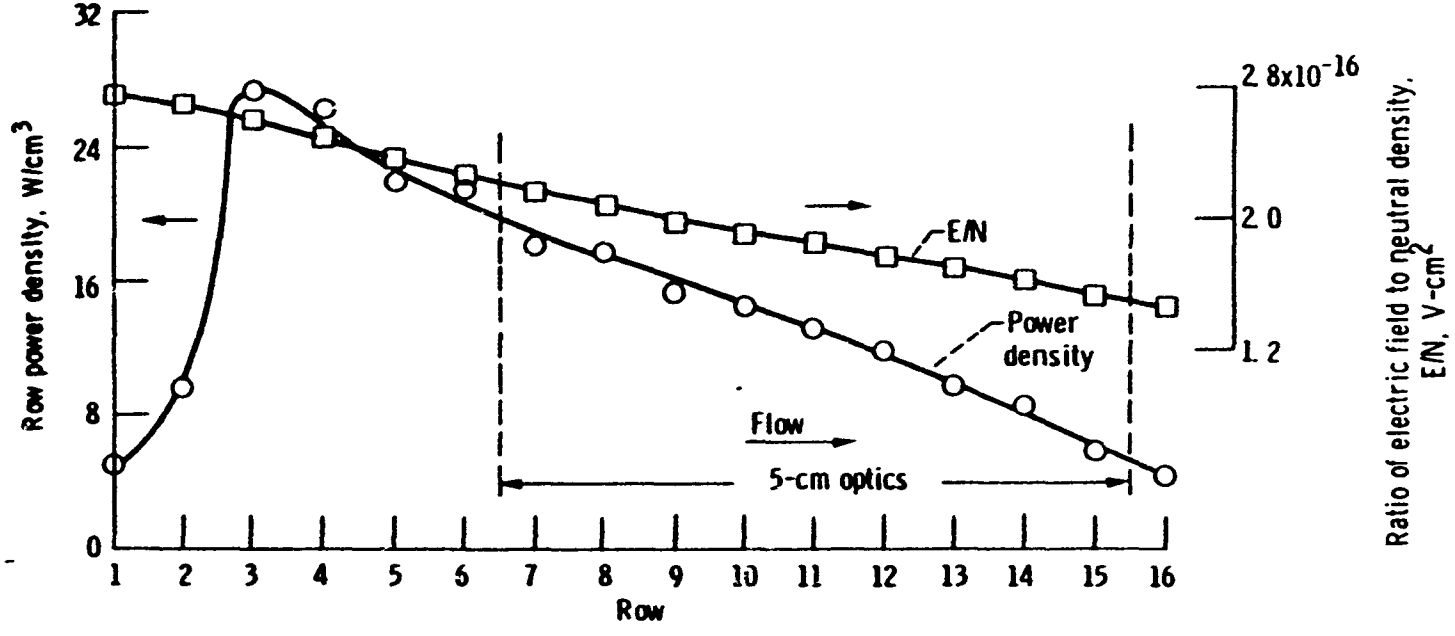

Discharge power density and distribution of ratio of electric field to neutral density. Laser power, 5.1 kW; discharge power, 74.0 kW; ballast power, 24.3 kW; total current, approximately 14.78 A; gas velocity, 104.9 m/sec; pressure. 147.3 torr [Ref. 18].

Figure 8

limited application and suffers from high cost, operating difficulties, and low power. The prime advantage is efficiency because of narrow bandwidth. The CO_2 lasers are "difficult to operate under normal circumstances" because they have a small gain coefficient on the lasing transition, but are scalable with pressure [Ref. 15]. A CO_2 laser pumped by a CO_2 laser on the 9P20 line has a laser efficiency of 14 percent [Ref. 16].

The answer to what method of pumping may be most efficient, reliable and cost effective will need more study. But ultimately, a system must consider these constraints as well as other factors such as turbulence and flows as parameters to be optimized. Turbulence in the cavity is undesirable for the laser light because of density fluctuations [Refs. 25 and 26]. But in electrical discharge convection lasers, the turbulence concurrently may permit more power into the discharge because of discharge stabilization which impedes the glow collapse (also known as plasma constriction of breakdown).

As stated earlier, this research centered on using electric discharges as a means of pumping the CO_2 laser. The electric discharge can be enhanced by convection and turbulence. Turbulence is the primary mechanism considered in the following section.

C. AERODYNAMIC STABILIZATION

To review, two methods of aerodynamic stabilization contribute to delaying the arcing or glow collapse and ultimate enchancement of power: convection and turbulence. Convection has been shown to control the discharge instabilities by cooling and removal of dissociated products [Ref. 5]. But convection may not only be used to remove the unfavorable chemical products, but also the unfavorable electrical products that cause early breakdown.

The mechanism of plasma constriction is not well understood, but the electrical instability problem is unique even though this problem "is due mainly to thermal effects," [Ref. 32]. Wasserstrom argues that an ionization increase results from lower gas densities caused by local uneven heating. A local current density then causes increased ohmic heating, more ionization, more current, until the instability is reached. Wasserstrom concludes that various flow configurations in gas lasers could be used to distribute the local heating effects homogeneously and thus postpone the glow-to-arc transition. He asserts that the flow configuration that will homogenize the hot spots is turbulence, but he continues, that with fast axial flows, convection can sweep away disturbances before they have a chance to grow [Ref. 32].

As mentioned earlier, convection's effects include both removal of dissociated products and cooling. Increasing

convection velocity reduces the residence time of the fluid in the cavity. Recall that residence time,

$$\tau_c = L_c/V_f \tag{15}$$

where L_c is the cavity length and V_f is the flow velocity. This reduction in residence time inhibits the formation of the discharge instabilities which result in constriction. Wiegand [Ref. 27] states that the plasma constriction instability plays a significant role in increasing discharge power density. The characteristic time for discharge instability formation is about 10^{-3} seconds. A typical residence time for one meter gap is 10 ms which is fast enough to remove the instabilities from the discharge.

To experimentally isolate the effects of residence time on power density, Wiegand kept the flow velocity constant in a non-turbulence discharge and varied only the gap length. A shorter gap corresponds to a shorter residence time. (The absence of turbulence is guaranteed by an unobstructed inlet and a length smaller than the 100 characteristic transverse dimensions required for the laminar to turbulent flow transition.) Constriction was found to be only weakly dependent on pressures over wide ranges as well as downstream gas temperature [Ref. 33]. By using successively shorter gap lengths, Wiegand recorded higher power densities

(Fig. 9). Wiegand concludes, "glow collapse does not occur until the power density reaches a value such that the growth time of the instability becomes comparable to the fluid residence time," [Ref. 27]. Maintenance of diffuse glow discharge at high pressures depends fundamentally on short residence time [Ref. 27]. Shorter residence times account for the increased power density observed by Barto in short gap, pin-to-plane discharges [Ref. 18].

The second major method of aerodynamic stabilization of the discharge is turbulence. Studying the effects of turbulence has been a continuing project at the Naval Postgraduate School under the supervision of Professor Oscar Biblarz. Power increases of more than 250 times the no flow conditions were observed by Nelson [Ref. 28]. Changes in the turbulence intensity spectrum has effects on the amount of power that could be coupled into the discharge [Refs. 11, 17, 18, 28, 29, 30].

In Eq. 10, the power is seen to be proportional to the gas pressure squared, but ionization is impeded as the pressure increases are continued and discharge stability problems are encountered. Barto [Ref. 18] discusses these effects and shows how an optimum pressure for a given cavity geometry can be derived.

Turbulence is known to have a profound time averaged effect on transport properties such as gas density and velocity. The time scales of turbulence are approximately

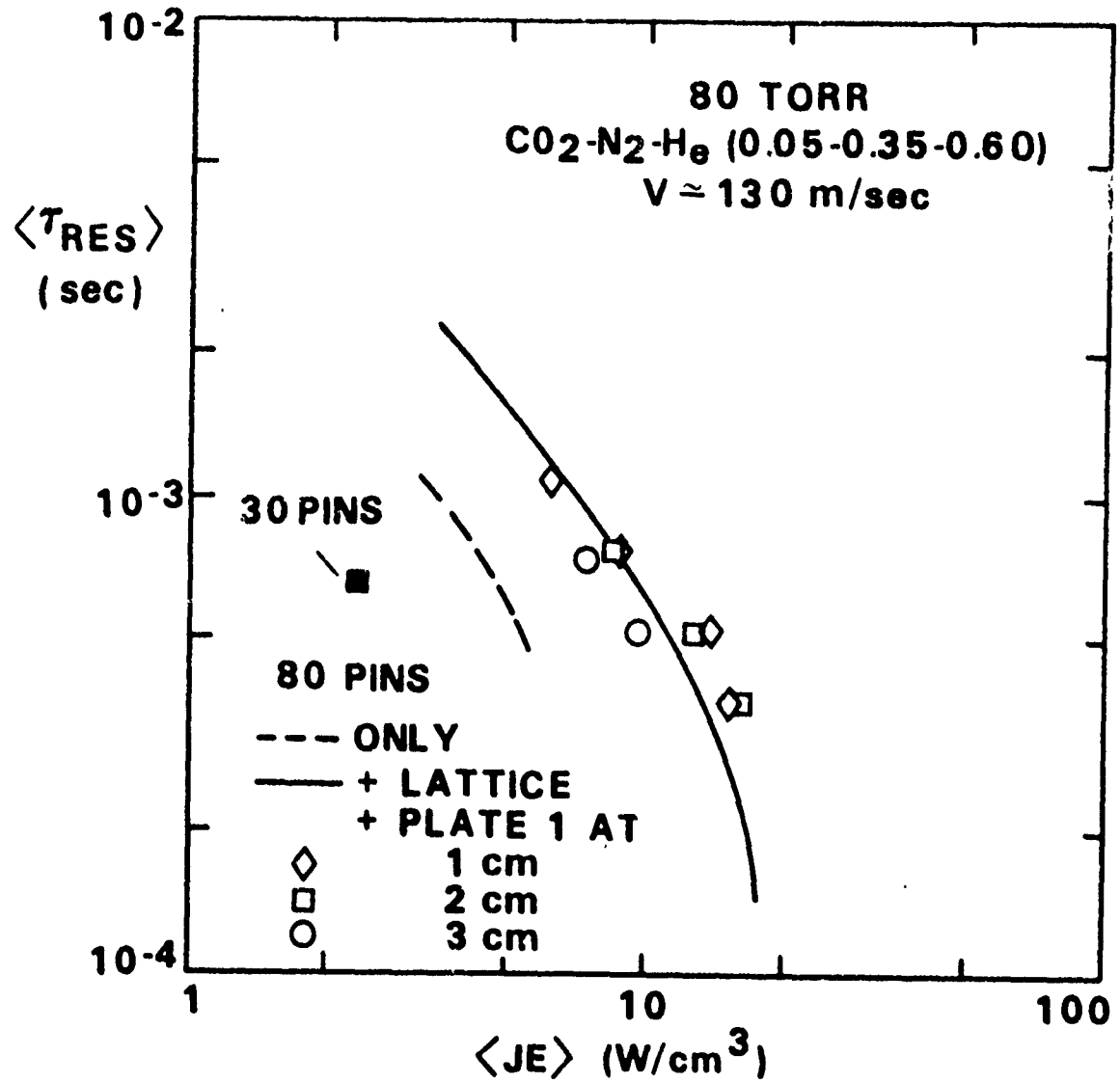

Fig. 9

Residence time versus power density in constant velocity and pressure with various electrode gaps and flow conditioner combinations [Ref. 27].

10^{-1} to 10^{-5} seconds, while the charged particle kinetics are much faster: ionization is 10^{-12} seconds, excitation is 10^{-12} seconds and streamer propagation is 10^{-8} seconds. Recombination is on the same order 10^{-5} to 10^{-6} seconds [Ref. 19] . Because of the different order of magnitude in time scales, turbulence can not directly affect the streamer propagation.

The interrelationship among current (power), ionization and turbulence can be postulated from the examination of

$$I = I_o e^{\alpha x_i} \tag{16}$$

where I is current, α now refers to the ionization and x_i is the point in the field where ionization begins to occur [Refs. 20, and 34]. The exponential dependence of current on the ionization is due to electron avalanche multiplication into the anode. This avalanche is responsible for the development of the intense ionization region at the anode which has been labeled "the anode extension" [Ref. 11]. The enhancement of ionization by turbulence can then be deduced from

$$\alpha = A(P + \Delta P)\exp[-B(P + \Delta P)/E] \tag{17}$$

where A and B are gas constants, E is the electric field and P is the time-varying pressure and ΔP is the change in

pressure. Due to the nature of this function the ionization is increased more by the negative fluctuations than by the positive fluctuations and more current is observed in a turbulent field with the average pressure equal to the pressure of the laminar convection field [Ref. 18]. Optimum pressures are not only a function of the convection, but are also controlled by the turbulence intensity and frequency which causes density fluctuations. For non-flow situations, an optimum pressure can be found for a given gas and electric field (Fig. 10) [Ref. 31].

The way in which the turbulence varies the power input to the cavity is not well understood and is complex as has been discussed. Experiments at the Naval Postgraduate School have centered around varying the turbulence spectrum throughout the cavity. Nelson found that by increasing the intensity of the turbulence at the lower end of the spectrum, below 1,000 Hz, more power could be coupled into the cavity. These turbulence spectra were varied by installing various turbulence generating screens upstream of the cavity [Refs. 17, 18, 29, 30]. Barto [Ref. 18] concludes that high intensity, low frequency turbulence is the best for stabilization. The greatest power densities were obtained for "Plate IX" which had a lower spectrum. Plate IX is a screen that was used by Post and Barto to generate turbulence. The variation in the plate's hole size and location can be compared in Figs. 11 and 12.

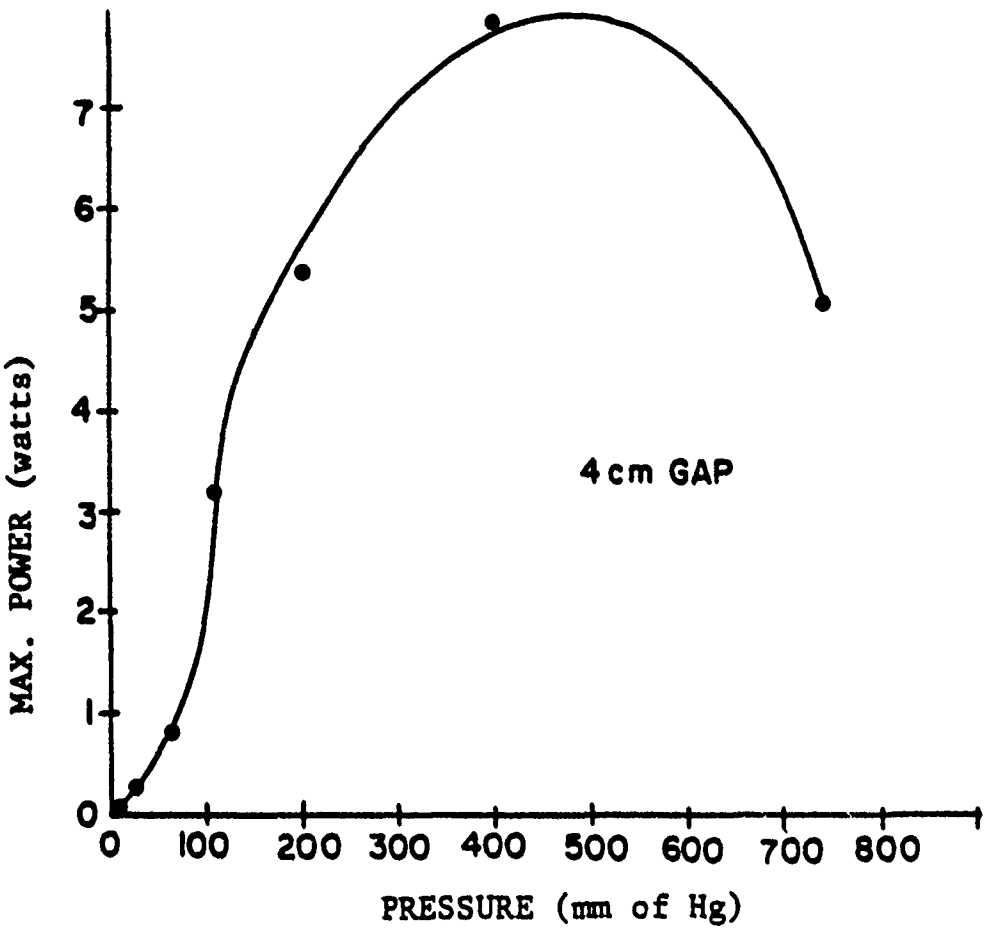

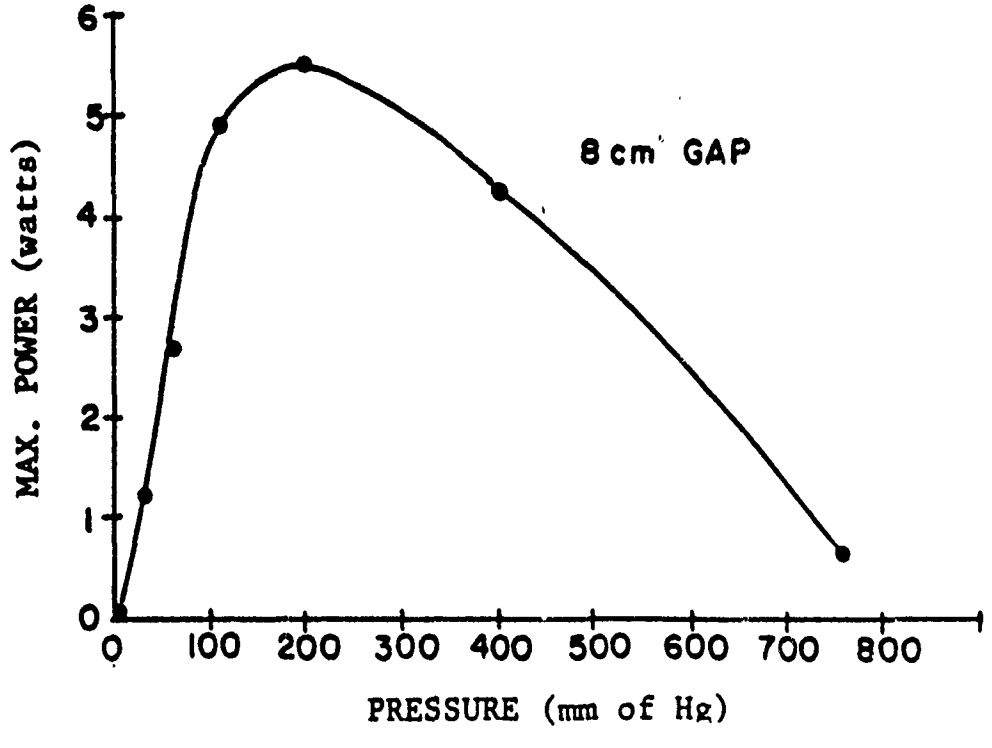

Fig. 10 Cavity power vs. pressure for no flow [Ref. 31].

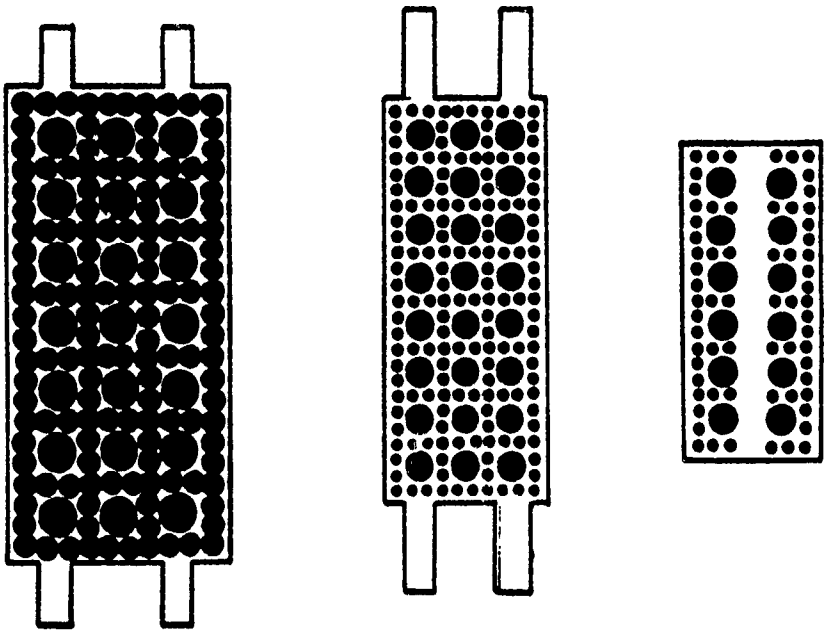

Plate I Plate II Plate III

	I	II	III
MATERIAL:	COPPER	PHENOLIC	ALUMINUM LAMINATED ON PHENOLIC
LENGTH (IN.)	6.0	5.2	3.6
WIDTH (IN.)	2.6	2.2	1.5
THICKNESS (IN.)	0.125	0.18	0.25
DIAMETER (IN.)			
LARGE HOLES:	0.50	0.375	0.375
SMALL HOLES:	0.187	0.125	0.125

Figure 11. Turbulence Generating Plates
[Ref. 30]

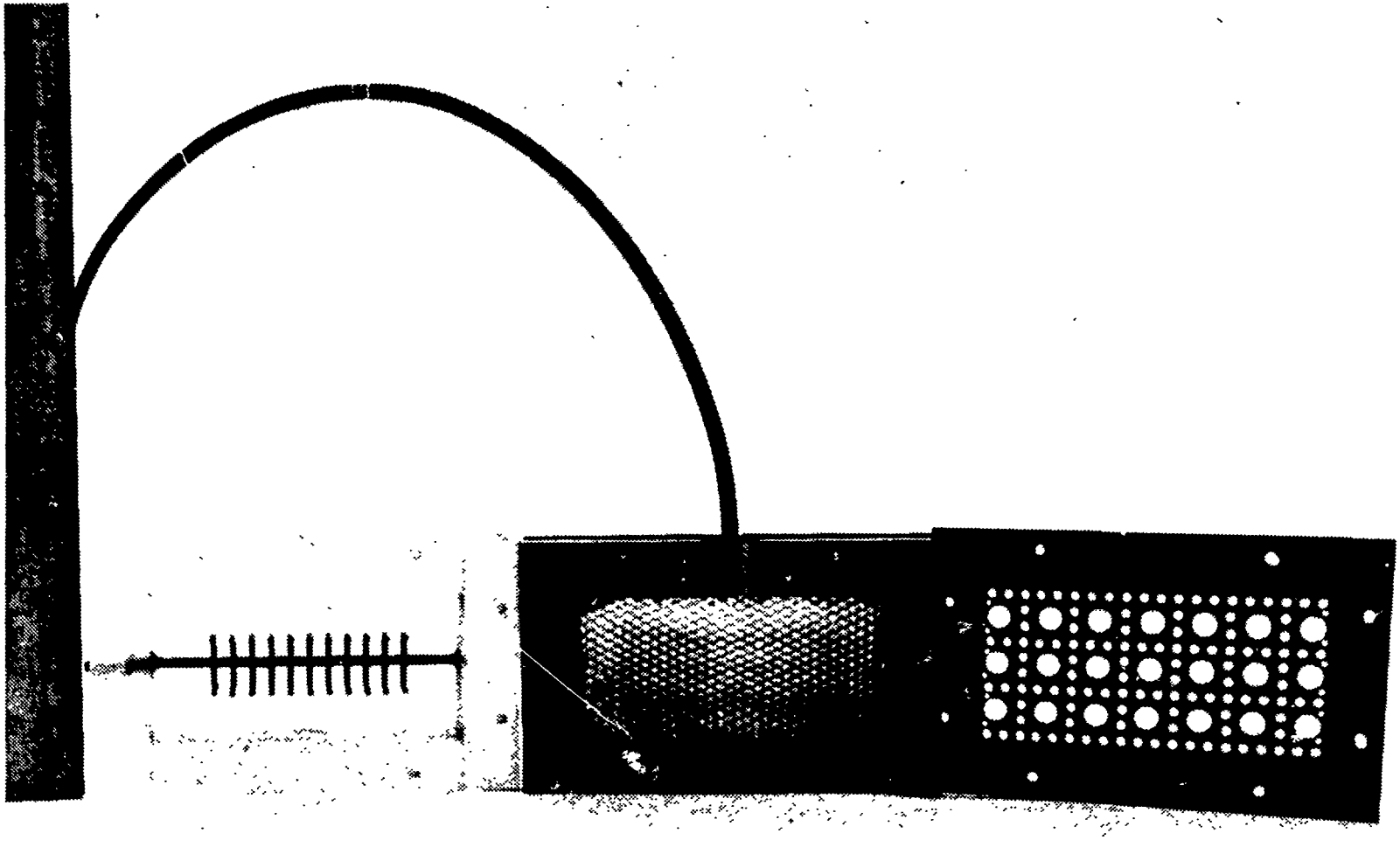

Fig. 12 Triple pin row anode, honeycomb cathode and Plate IX of Post and Barto's set-up

The disadvantages of arranging plates or screens upstream of the cavity are that high back pressures reduce the flow and that changing screens to investigate the effects of different spectra is time consuming and expensive in engineering. The effect of the screens appears to be self-limiting due to their inabilty to generate intense eddies in the range from 100 to 1000 Hz. For this reason, a secondary flow with a triple slot was designed and mounted upstream of the cavity (Figs. 13, 14). This arrangement is in effect three unsteady jets, which are known to increase the mixing rate in a flow through turbulence [Ref. 21]. The oscillator arrangement incorporates the ability to change the spectrum and emphasize certain frequencies which is not possible using screens.

The mixing is accomplished through a gross disturbance of the jets which lengthens the interface and enhances the entrainment. The entrainment region of pulsed, subsonic jets is a region of intense turbulence. Pulsed ejector mixing is accomplished by free-jet-boundaries of free-turbulent flows. (Whereas, a grid-generated turbulence as developed with the screens is turbulence generated along the walls.) The mixing length is assumed to be proportional to the width of the jet and is a constant value. In Fig. 15, the growth of the mixing area is shown [Ref. 23]. The rate of change of the width is proportional

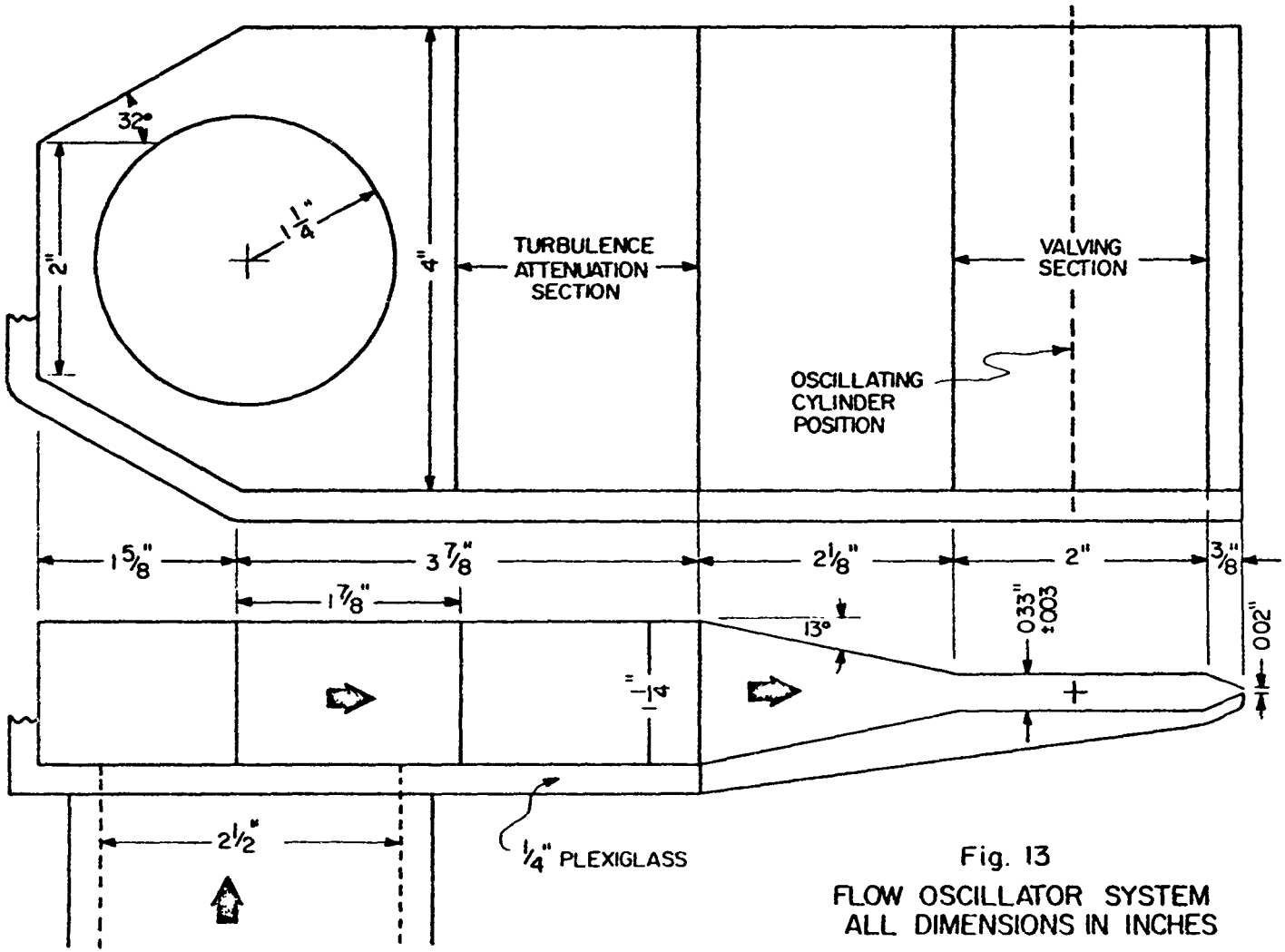

Fig. 13
FLOW OSCILLATOR SYSTEM
ALL DIMENSIONS IN INCHES

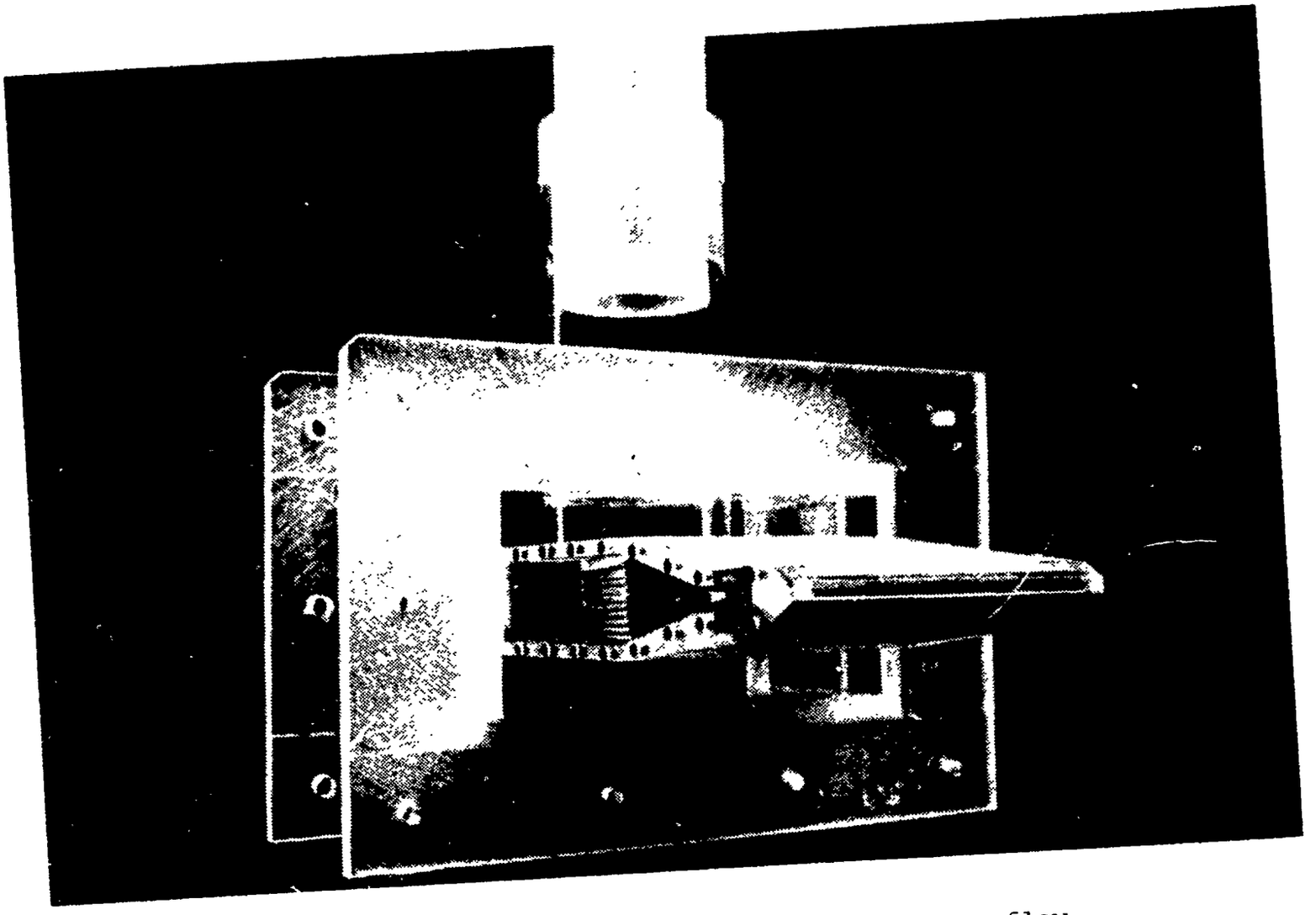

Fig. 14 Secondary flow positioned inside primary flow. Honeycomb flow straigthener is barely visible in secondary flow.

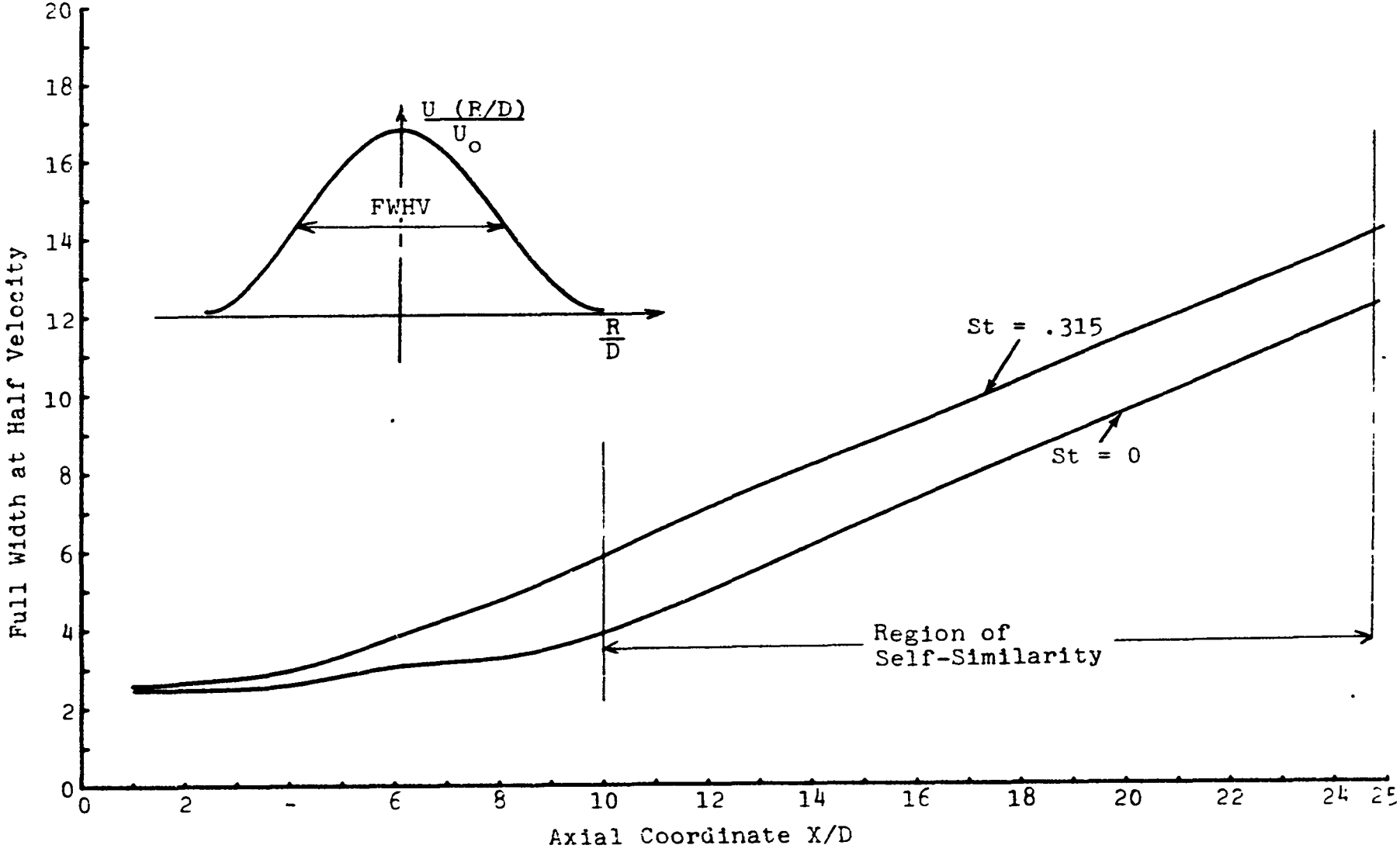

Fig. 15 Growth of Ejector of Mixing Area [Ref. 23]

to the tranverse velocity, which can be scaled by the turbulence frequency.

The way the transverse velocities arise is best explained by an example. Recall from boundary layer theory in two dimensional flow that the fluid's velocity is slower along the wall and faster at points away from the wall. By convention, x represents the distance along the wall in the direction of the flow and y the distance away from the wall. Velocities in the x direction are u' and velocities in the y direction are v'. It may be imagined that the transverse velocity fluctuation orginates in the following way: Consider two lumps of fluid meeting in a lamina at a distance y_1, the slower one from $(y_1 - \ell)$ preceding the faster one from $(y_1 + \ell)$. In these circumstances the lumps will collide with a velocity 2 u' and will diverge sideways. This is equivalent to the existence of a transverse velocity component in both directions with respect to the layer at y_1. If the two lumps appear in the reverse order they will move apart at a velocity 2 u' and the empty space between them will be filled from the surrounding fluid, again giving rise to a transverse velocity component in the two directions at y_1. This argument implies that the transverse component v' is of the same order of magnitude as u' and we put, [Ref. 35].

$$v' = \text{const} \tag{18}$$

$$u' = \text{const} \cdot \ell \frac{du}{dy} \qquad (19)$$

The larger the difference in the two flow velocities, the larger is the transverse velocity and more turbulence and mixing results. Optimum mixing efficiency is obtained when the mass flow rates are equal. The gross disturbance, in these experiments, was caused by a rotating cylinder in the jet. The cylinder has an egg-shaped cross-section which, when rotated, alternately passes and restricts the flow. More intense oscillations have higher spreading rates as seen in Eq. 18 and 19. An optimum frequency for the pulse jet oscillations can be found in terms of mass flow of the primary mass flow to the secondary mass flow which is alternating. As is well known from ejector principles, for a given primary flow there is a secondary flow (Fig. 16) energy input that gives a most efficient spread and turbulence intensity [Ref. 22].

With this pulsed jet, the eddy sizes can be varied by changing the pulses of the jet. Viets [Ref. 23] shows that maximum mixing is achieved from a sine wave oscillation. For a given set of flow conditions, a single oscillation frequency will produce an optimum mixing. By incorporating a method of pulsing the secondary flow and by having the ability to change the frequency for different flow conditions, a wide variety of turbulence spectra and

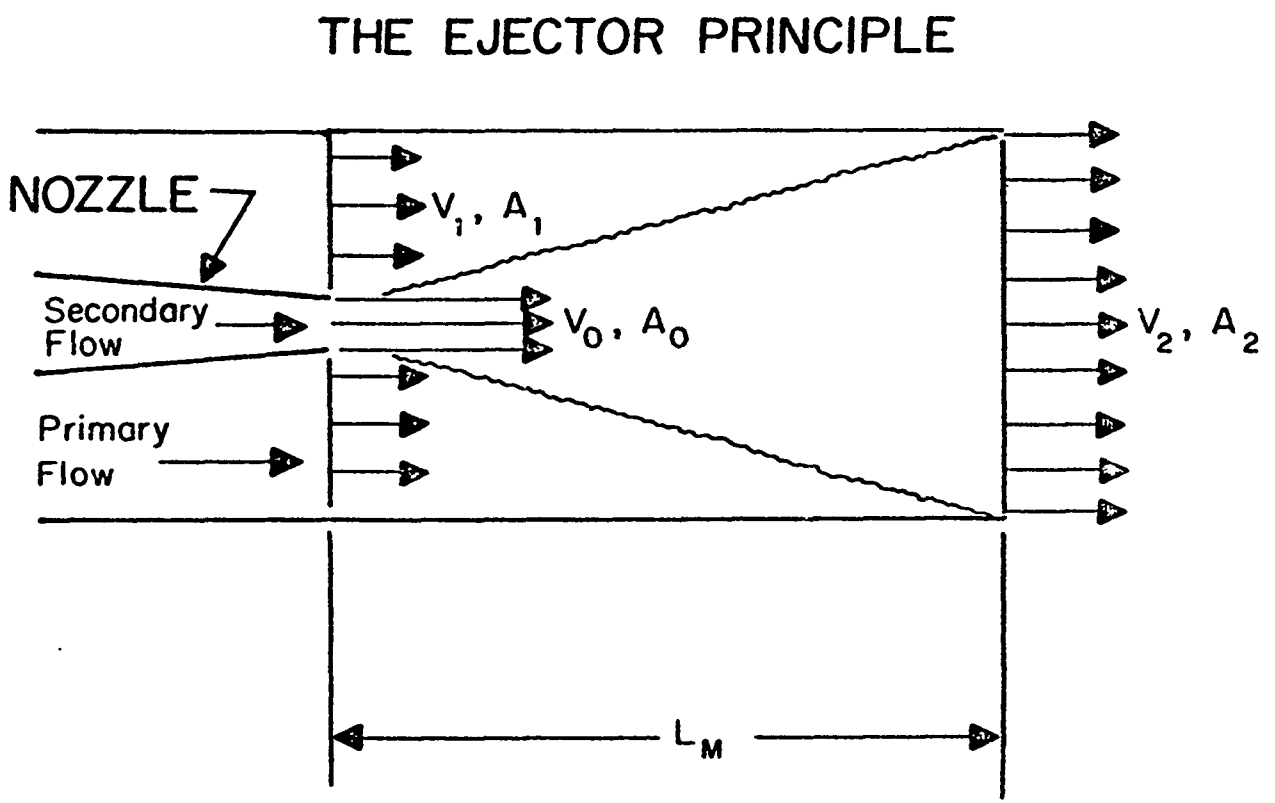

Fig. 16 The Ejector Principle

intensities may be investigated without changing the experimental set-up.

Another method of turbulence generation, which has back pressures lower than those associated with grid generated turbulence, is to mount "mini-plates" on the anode (see Fig. 17) that will trip the laminar flow on the pins [Ref. 36]. This set-up is believed to provide the turbulence spectrum required in the discharge region because of the proximity of the turbulence generation to the pin tips -- the place that the turbulence appears to be needed most. The nearness of the eddy generation permits a weaker turbulence to be generated by the grid because it cannot decay significantly before reaching the pin-tips. Savings in flow power were expected from this arrangement since the blockage is minimized. However, the "mini-plates" may cause a signficant velocity defect at the pin-tips. This velocity defect is thought to be caused when the "mini-plate" is mounted to close to the anode tip. There is apparently some flow blockage in the region directly downstream of the "mini-plate", even with the small holes in the "mini-plate". This velocity defect may be the cause of the reduced turbulence intensity at the anode tip. This problem is addressed in more detail in Sec. V.

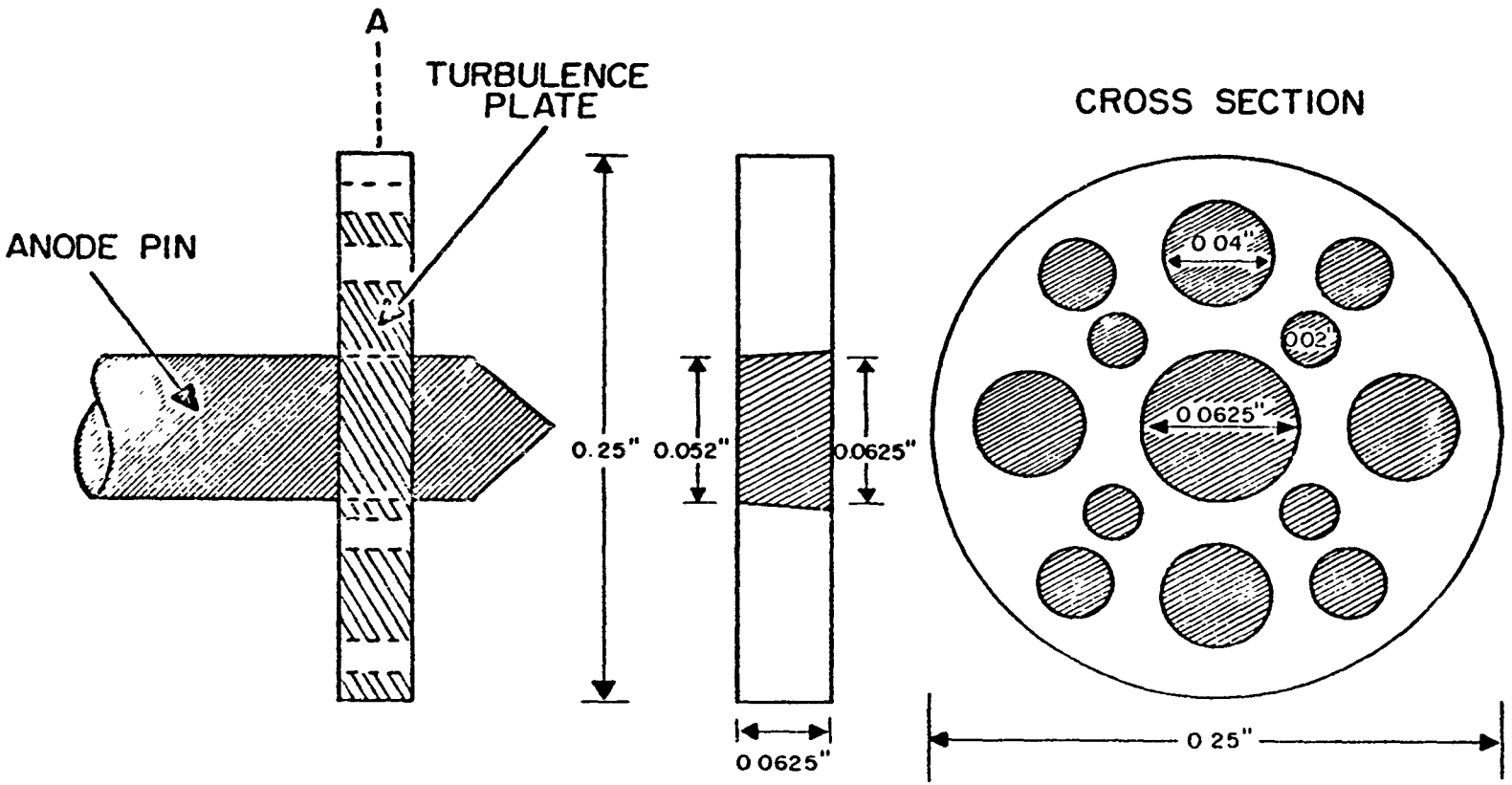

Fig. 17 Phenolic Turbulence Generating Plates Mounting Close to Electrode Tip.

II. SYSTEM DESIGN

The system design was an extension of the system originated by Post [Ref. 30]. The diffuser, however, was not mounted which resulted in a converging nozzle (replacing a converging-diverging nozzle) feeding into a constant area duct, in which the test cavity is located. A secondary flow source was mounted in the converging section of the nozzle to minimize the blockage of the flow while maximizing the effectiveness of the oscillator in the secondary flow (Figs. 18 and 19). The minimal blockage lowered the back pressures that were experienced with turbulence generating screens mounted in the flow in Refs. 17, 18, 28, 29, 30 and 34. (The screens had produced up to fifty percent area blockage to the flow.)

As implied above, the oscillator jet output had to be located in the constant area section to be most effective. The oscillator was to be employed in generating low frequency, high energy turbulence. This type of turbulence is rapidly attenuated by the accelerating flow in the wind tunnel contraction, called vortex stretching. Furthermore, to minimize the effects of turbulence decay, the jet would be mounted close to the cavity while still allowing for the length required for full development by entrainment. The jet design is two dimensional and mixing is primarily in one (and not both) of the cross flow dimensions. This seemed

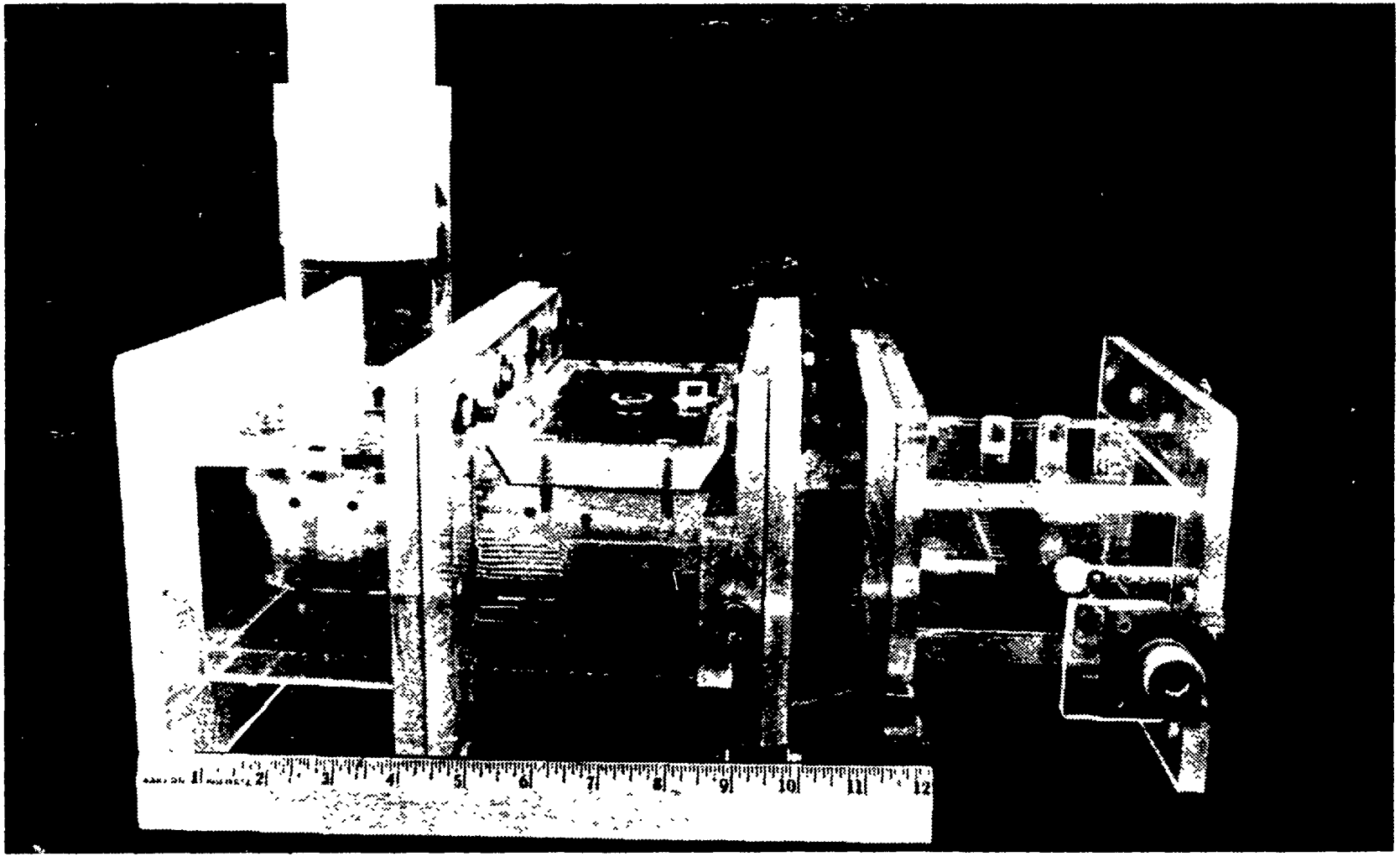

Fig. 18 Primary and Secondary Flow Confluence, Converging Nozzle and Test Cavity

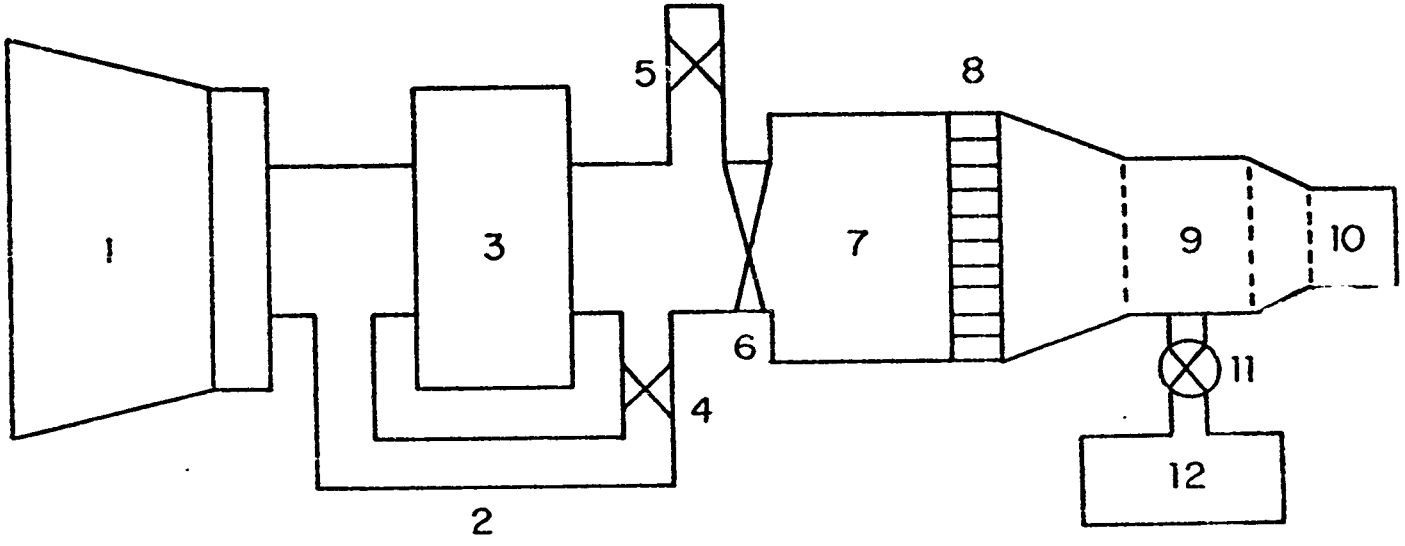

1. Compressor (Primary)
2. Heat Exchange By-Pass
3. Heat Exchanger
4. Gate Valve
5. Gate Valve
6. Gate Valve
7. Plenum (Particle Precipitator)
8. Honeycomb
9. Plate Chamber
10. Test Section
11. Diaphram Throttling Valve
12. Storage Tank (Secondary)

Fig. 19 Flow system schematic

reasonable given the "two dimensionality" of the electrode configuration.

Because maximum mixing intensity is desired in the discharge cavity, a sinusoidal pulsing of the secondary flow was the design goal of the oscillator. Bremhorst and Harch [Ref. 37] describe a pulsating valve consisting of synchronized rollers, modified to form a cylindrical passage during part of their cycle of rotation. Bauman [Ref. 38] reports on the development of a control valve for the production of an oscillating flow. Bauman's cylindrical flow passage was valved with an elliptical lucite cam designed to produce a real sinusoidal flow. The real flow effects of Bauman's design were observed in the laboratory by Biblarz [Ref. 41] to produce sinusoidal flow outputs. Cam rotating frequencies of from 50 to 80 Hz yielded relatively pure sinusoids.

Prandtl [Ref. 35] and others have shown that a rotating cylinder is effective in preventing separation of the boundary layer. When the cylinder is not rotating, vorticity will be shed at the Strouhal frequency from the separation region, as a result of boundary layer effects. This shedding is asymmetric and continues as the boundary layer grows. For given rotation of the cylinder, the upper relative velocity will increase causing the boundary layer to grow in length due to the effects of the Reynolds number.

In this intermediate condition, two frequencies of turbulence will be generated, one above and the other below the Strouhal frequency. As the cylinder rotation velocity increases for a given channel flow rate, the upper and lower separation regions merge giving rise to nearly potential flow which results from reduced losses [Refs. 35 and 39]. To further diminish the effects of shed vorticies, the present oscillator design positioned the rotating cylinder upstream of the converging accelerating secondary flow to employ the turbulence damping of vortex stretching.

Separation behind the ellipsoid and the resulting eddies are problems of Bauman's valving concept, but in this lower frequency range, adverse pressure gradients do not develop well and the separation is minimal. To enhance turbulence intensities below 1000 Hz, rotating cylinder frequencies of up to 100 Hertz are required. (Turbulence generating grids and screens have been unable to generate high intensity turbulence below 100 Hz.) The pulsing introduces intensities of decaying value at integer multiples of the oscillating frequency. These spikes of flow power at the multiple frequencies are called overtones.

To enhance these lower frequencies and hopefully stabilize the discharge, an egg-shaped cylinder was designed to be positioned in the secondary flow (Fig. 20). The profile was designed and manufactured according to the following equation:

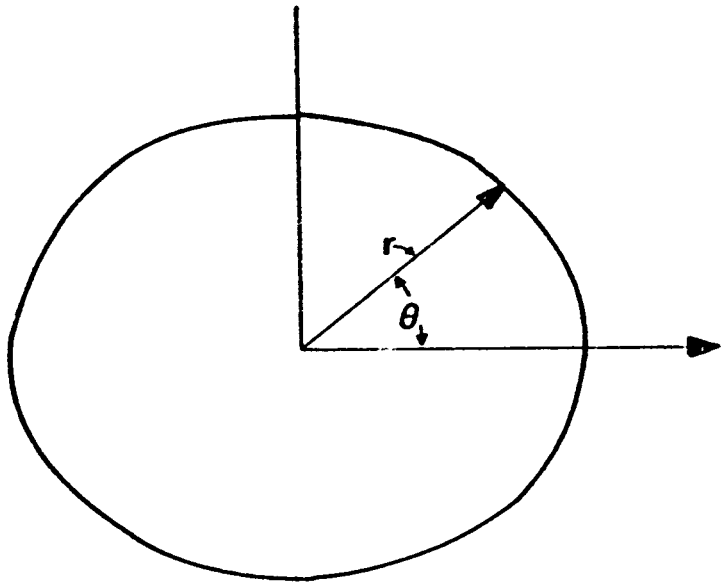

$r(\theta) = 0.150 - 0.025 \sin\theta$ (Inches)

Fig. 20 Cylinder Cross-Section

$$r(\theta) = 0.150 - 0.025 \sin \theta \text{ (inches)} \qquad (20)$$

A small space was given to the maximum blockage of the cylinder in the secondary flow to accommodate the engineerng tolerance of plexiglass.

Final design modification of Post's apparatus was to reduce the number of pin rows from three to one, and to remanufacture the cathode grid for strength and better spacing control. The existing grid had bowed due to the high flow velocities and preferential arcing had been observed. The single pin row, while also reducing the risk of preferential breakdown, made maintenance of homogeneous flow an easier engineering problem without sacrificing the significance of the results (Fig. 21).

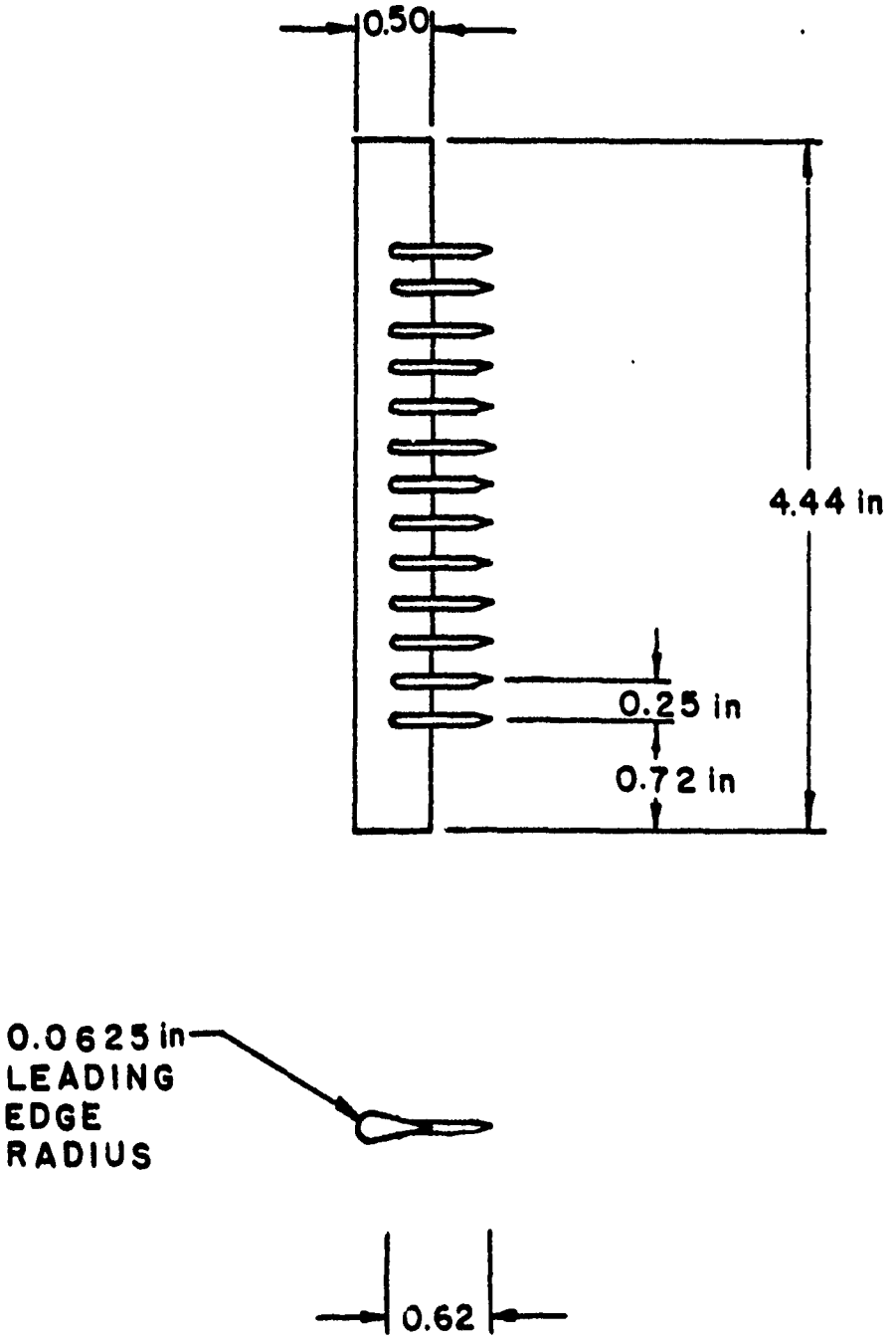

Fig. 21 Anode Single Pin Row Design

III. EXPERIMENTAL APPARATUS

The experimental apparatus has three major subsystems. These include two air supplies, a variable high-voltage DC discharge circuit, and a turbulence measurement set-up. There are many similarities between this set-up and the one used by Post and Barto [Refs. 18, 30].

A. FLOW SYSTEMS

The flow systems consist of two compressors with associated heat exchangers and flow rate control valves and a storage tank, a plenum and converging nozzle, and a pulsed jet ejector flow (Fig. 19). The primary air supply is provided by a Carrier three-stage centrifugal compressor with a 4000 ft^3/min capability at a maximum pressure of two atmospheres. The flow is directed through a water-cooled heat exchanger that maintains a stabilized flow temperature at 90° F.

Three gate valves control the flow rate into the converging nozzle and test cavity. Two valves are located downstream of the heat exchanger and are the primary control valves. A bypass valve has been installed ahead of the heat exchanger to eliminate chocked flow in the exchanger at maximum flow rates. Aluminum honeycomb, installed ahead of the converging nozzle in the primary flow, dampens upstream

turbulence generated in the plywood plenum. The plenum has a particle precipitator.

The secondary flow is provided by a 300 psi storage tank which is pressurized through a dryer from a Sullivan compressor. This flow is controlled by a diaphragm throttling valve and is measured between the valve and the oscillator in gage pressure. The converging nozzle, oscillator and test cavity are manufactured from plexiglass and is the area where the two flows merge (Fig. 18).

B. THE DISCHARGE CIRCUIT

With the exception of the electrodes, the discharge circuit is identical to the circuit used by Post and Barto [Refs. 18 and 30]. A Sorensen Beta high-voltage, DC power supply with a rated maximum output of 60 kV and 60 mA was used, although only 30 kV and 20 mA were actually available.

The test cavity incorporates the anode and cathode (Fig. 22). The grid wires replaced with thin brass strips are stronger and actually present less cross-sectional area to the flow. The cathode gap can be adjusted from one to three centimeters. The turbulence "mini-plates" were manufactured from phenolic and friction fit so they can be adjusted to various positions on the anode pin (Fig. 17).

C. TURBULENCE AND OTHER DIAGNOSTIC EQUIPMENT

The only addition made to the diagnostic equipment of the Post and Barto [Refs. 18 and 30] set-up was a miniature

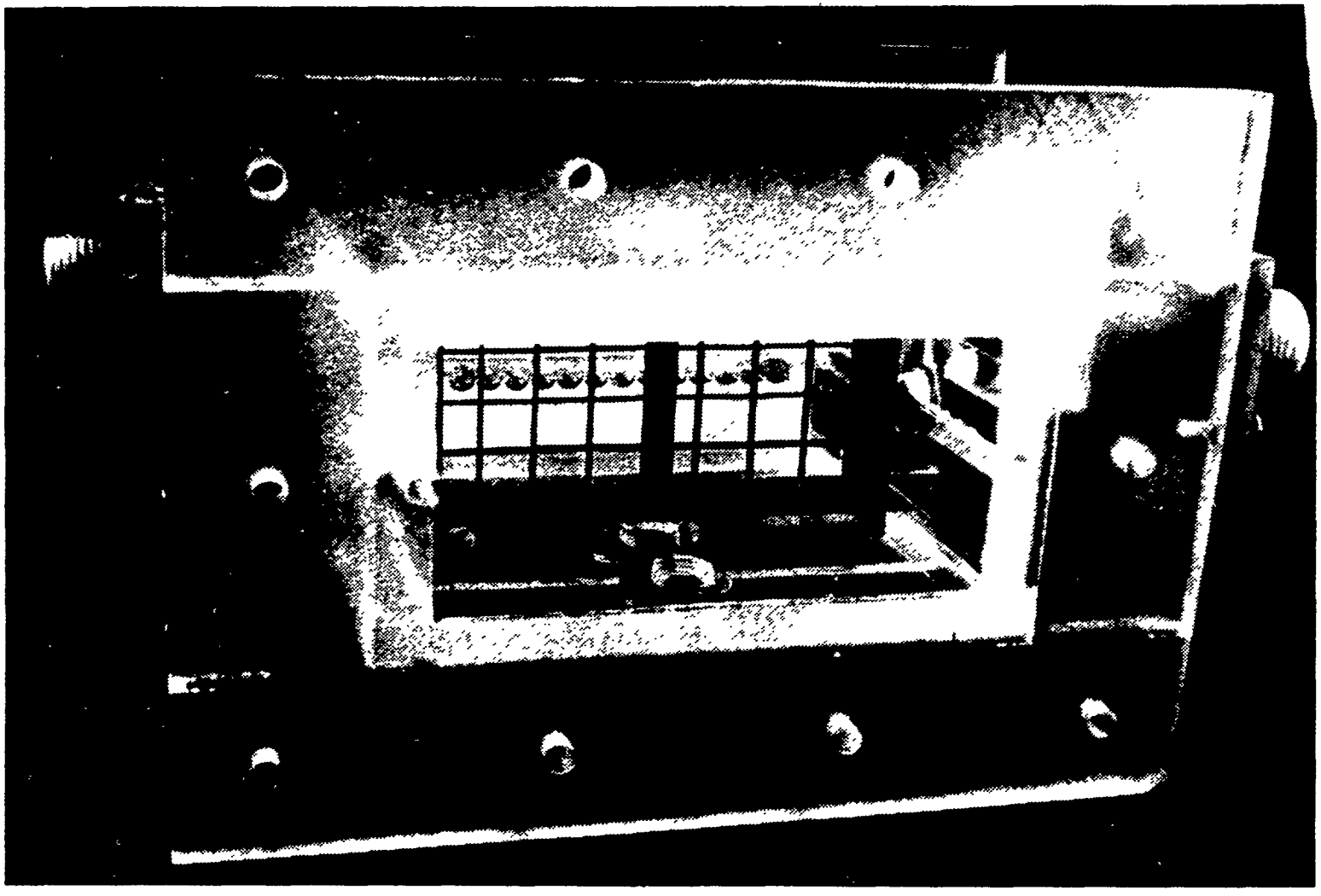

Fig. 22 Test Cavity Close-up. Single Pin Row Anode with "Mini-plates" visible behind cathode.

piezoresistive pressure transducer, Endevco Model 8507. The transducer is used to measure the fluctuations in pressure, i.e., the turbulence intensity and frequency in the cavity. This instrument had the advantage of being more rugged than the conventional hot-wire anemometers normally used to measure these data.

The active area of the pressure sensing surface is silicon semiconductor, 2 mm in diameter. A Wheatstone bridge is diffused into the silicon. The stress variations are concentrated at the resistive elements which results in a sensitivity rivaling the anemometer [Ref. 40]. The transducer was found to have adequate linearity, frequency response and noise rejection characteristics. Several lower flow velocity runs were used to directly compare the hot-wire anemometer and pressure transducer systems. In Fig. 23, different modes of turbulence are shown for the transducer readout on the spectrum analyzer. Information representing the turbulence intensity and frequency was taken from the pressure transducer, amplified and input to the spectrum analyzer. The analyzer then divided the signal strength into frequency components from 0 to 20 kHz. The frequency spectrum was displayed on an X-Y recorder on a log - log scale. The spectrum analyzer used was a Spectra Dynamics Corporation Model SD 330 Spectra Scope and the X-Y recorder was a Hewlett Packard 7035B X-Y Recorder.

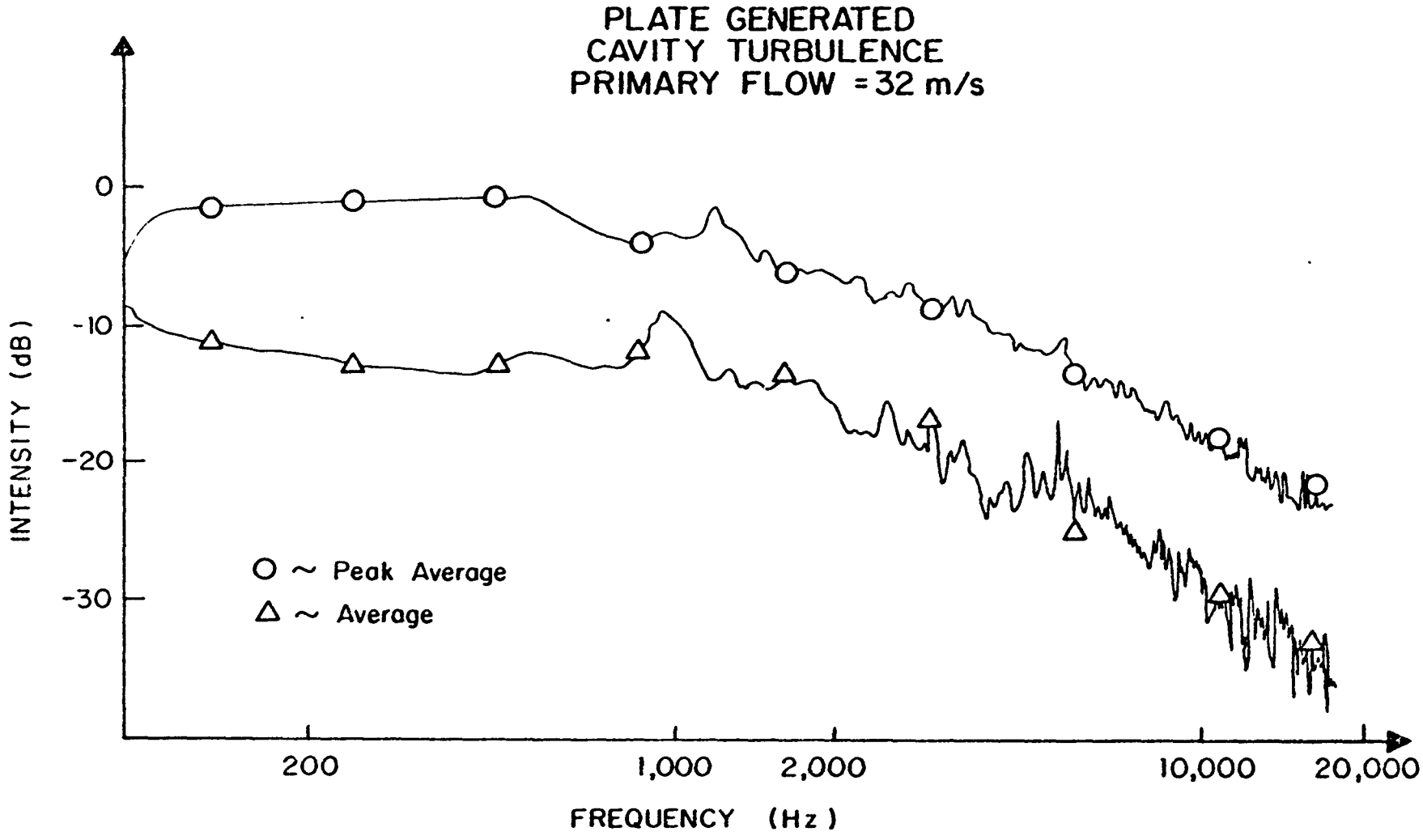

Fig. 23 Turbulence Spectra Average Comparison

IV. METHOD OF INVESTIGATION

From previous investigations, higher power inputs are thought to be associated with turbulence spectra that are more intense at lower frequencies [Refs. 11, 17, 30, 34]. Furthermore, the turbulence generated by Plate IX was found to have the highest power input coupling of the plates tested for reasons that were not immediately clear.

Two basic measurements of discharge performance are needed. A primary interest in the amount of power that can be coupled into the discharge before the glow collapse requires the measurement of current and voltage. Next, the turbulence spectra associated with these power inputs would have to be known. As was later discovered, not only is there interest in keeping the turbulence three dimensional and uniform across the anode pins (in a plane normal to flow), but the way the turbulence grows and decays while transiting the cavity is also very critical.

A. TURBULENCE TESTS

Using the pressure transducer with the spectrum analyzer and an X-Y recorder, the first objective was to determine exactly which of the lower turbulence frequencies could be enhanced by various flow parameters and RPM settings of the oscillating cylinder. Also, for increasing flow rates the

determination that the turbulence was fully developed and that it filled the test section was carried out by taking readings at the top and bottom reading at the top and bottom corners of the test cavity. For primary flows of up to 110 m/s and secondary flows up to 70 m/s, the entrainment region was found to be long enough to permit the full development of the pulse generated turbulence throughout the cavity. The turbulence was found to stay fully developed and homogeneous 5 cm beyond the anode plane. For this reason, spacers, which were originally designed to lengthen the entrainment region, were not used. Oscillator-generated cavity turbulence is recorded in Figs. 24, 25, 26, and 27. In Fig. 28, oscillator turbulence before the cavity shows the harmonic overtones of the frequency generated by the rotating cylinder. The results in these figures are discussed in Sec. V.

Turbulence spectra (Figs. 29 and 30) were also taken for the "mini-plates" and were found to be homogeneous across the anode region, but not fully developed in the region of the positive space charge when the "mini-plates" were mounted on the anode tips. The turbulence generated with the "mini-plates" at the anode tips became fully develped at 0.5 cm into the gap and maintained this intensity to 2.5 cm and beyond. Turbulence spectra of Plate IX from Barto and Post's work were also examined. This required removing the two-flow apparatus (Fig. 18) and installing the converging

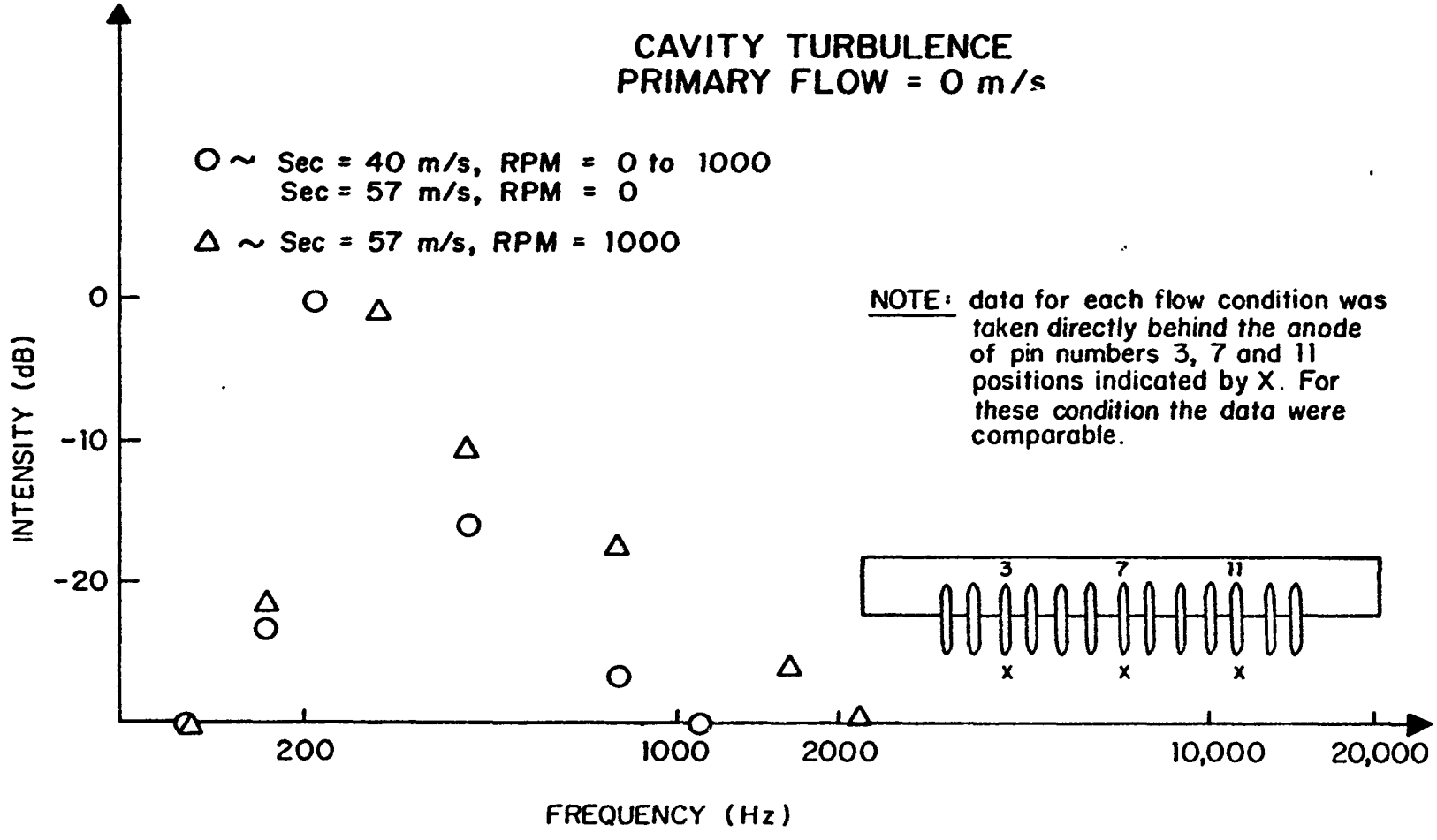

Fig. 24 Turbulence Spectra

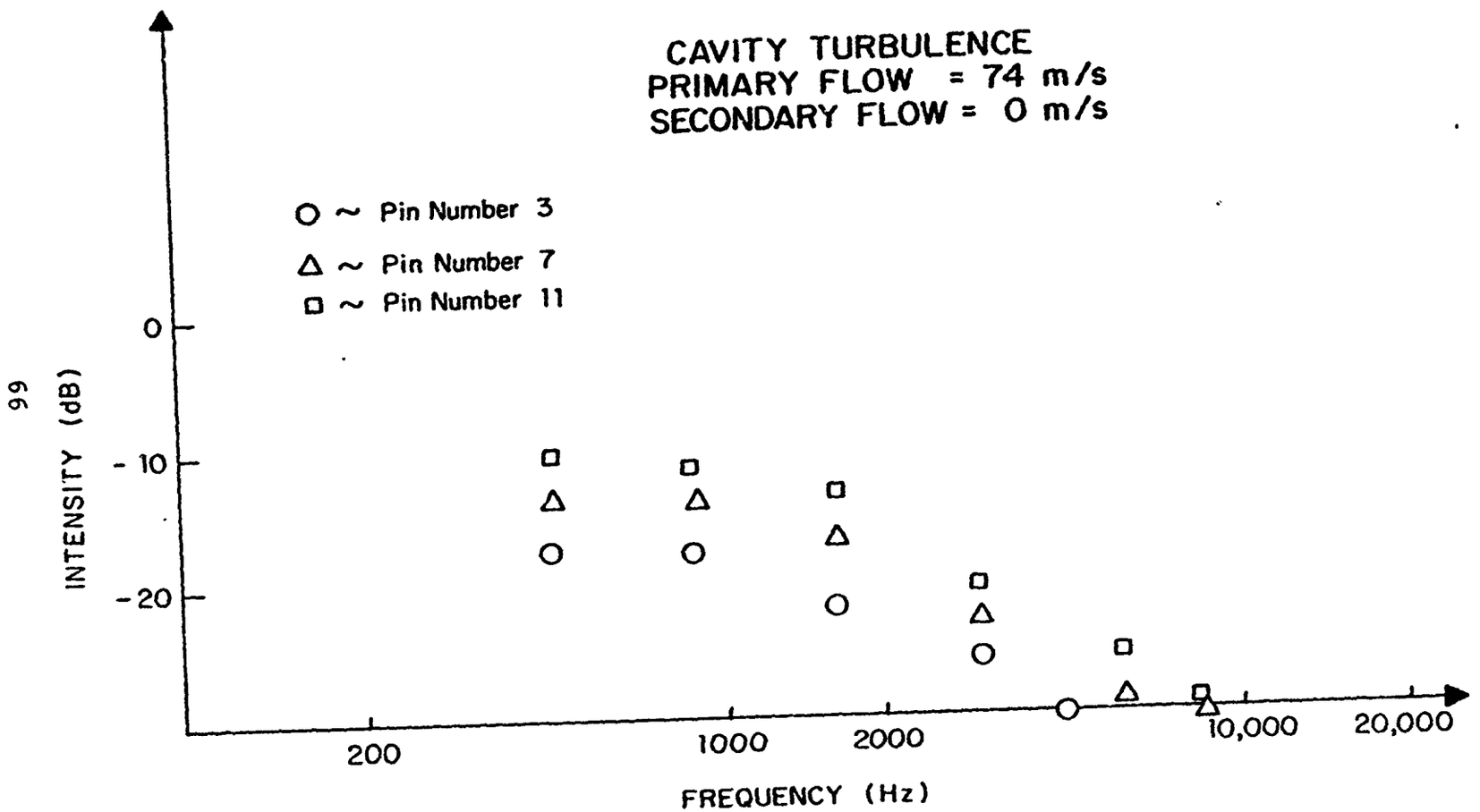

Fig. 25 Turbulence Spectra

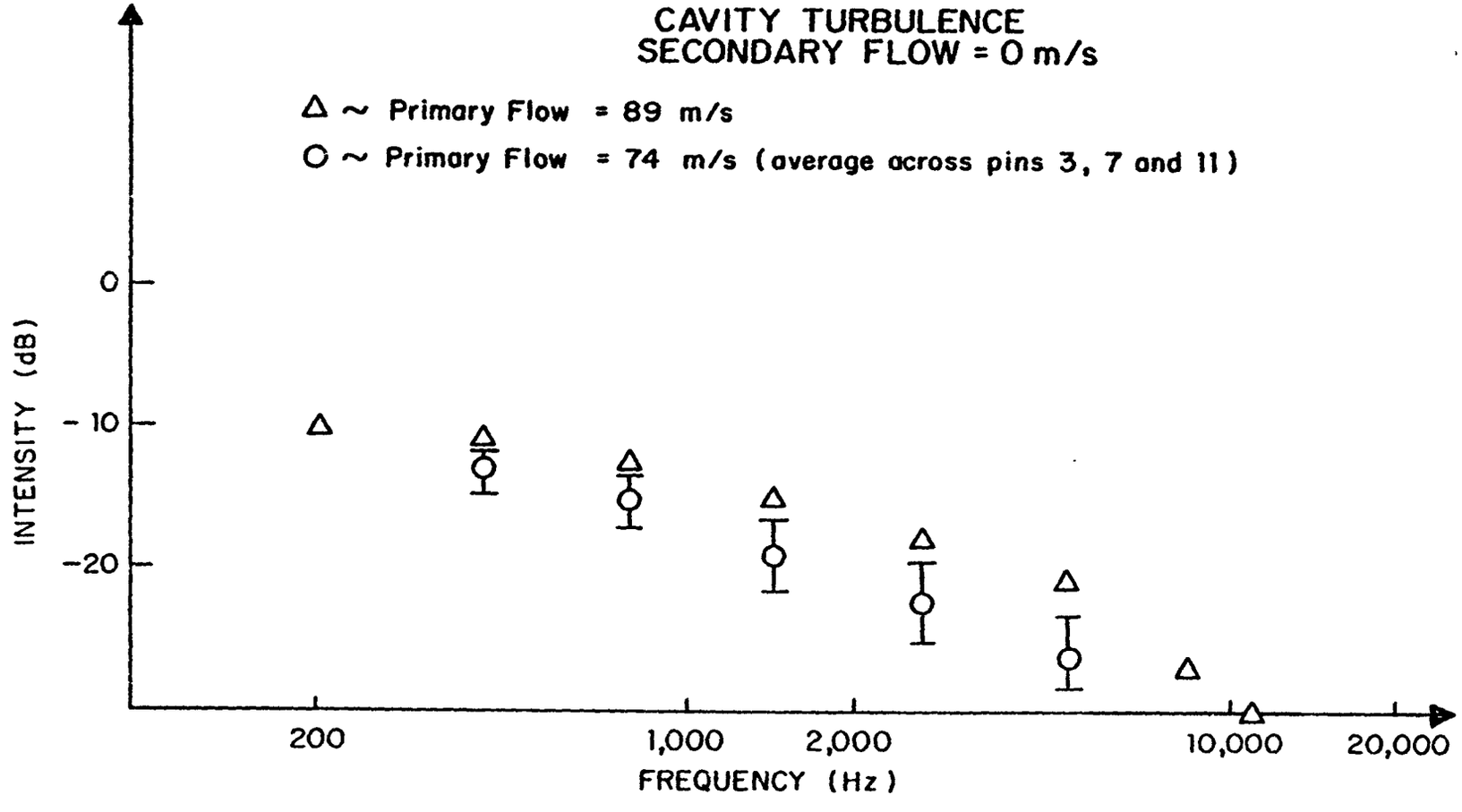

Fig. 26 Turbulence Spectra

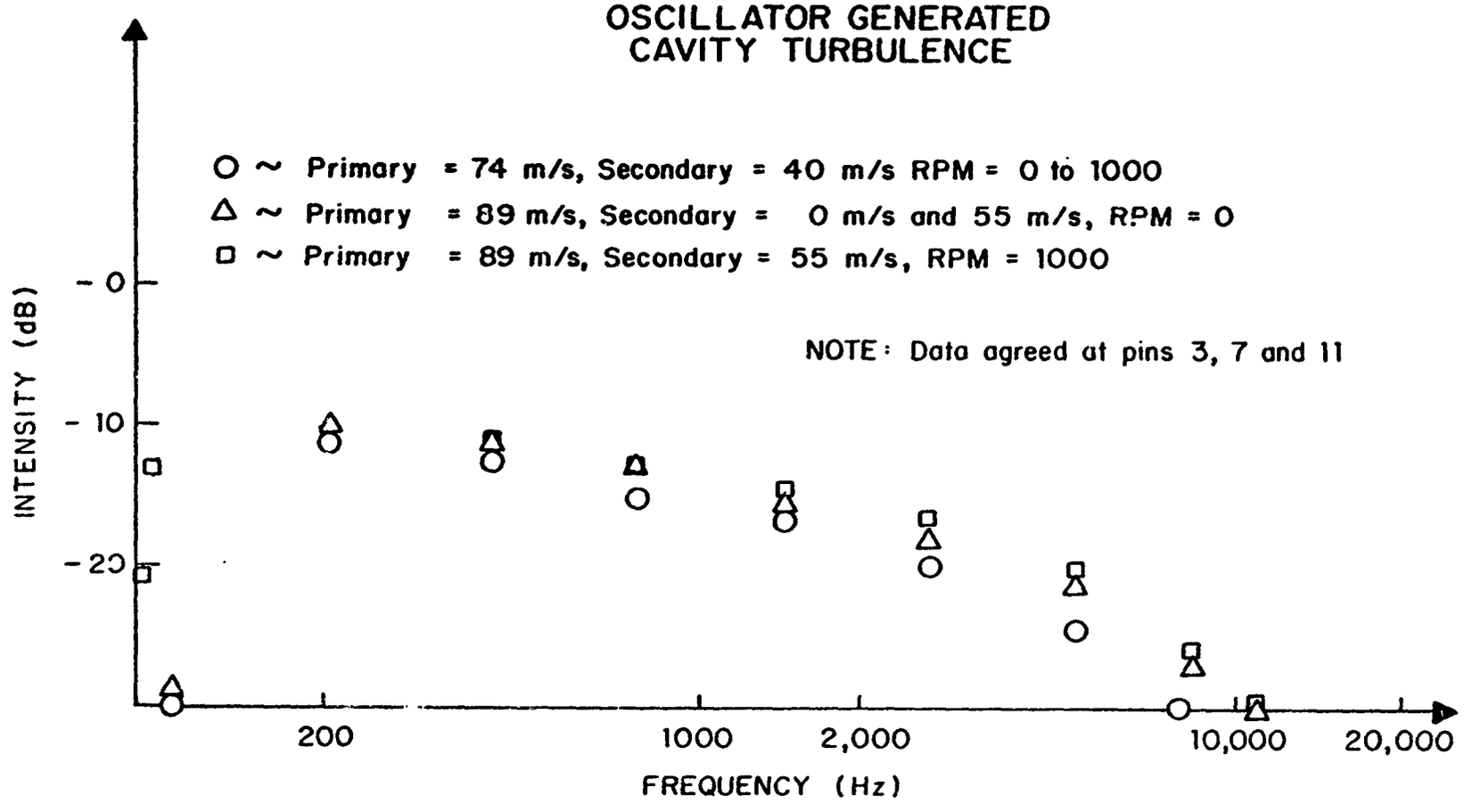

Fig. 27 Turbulence Spectra for Oscillator

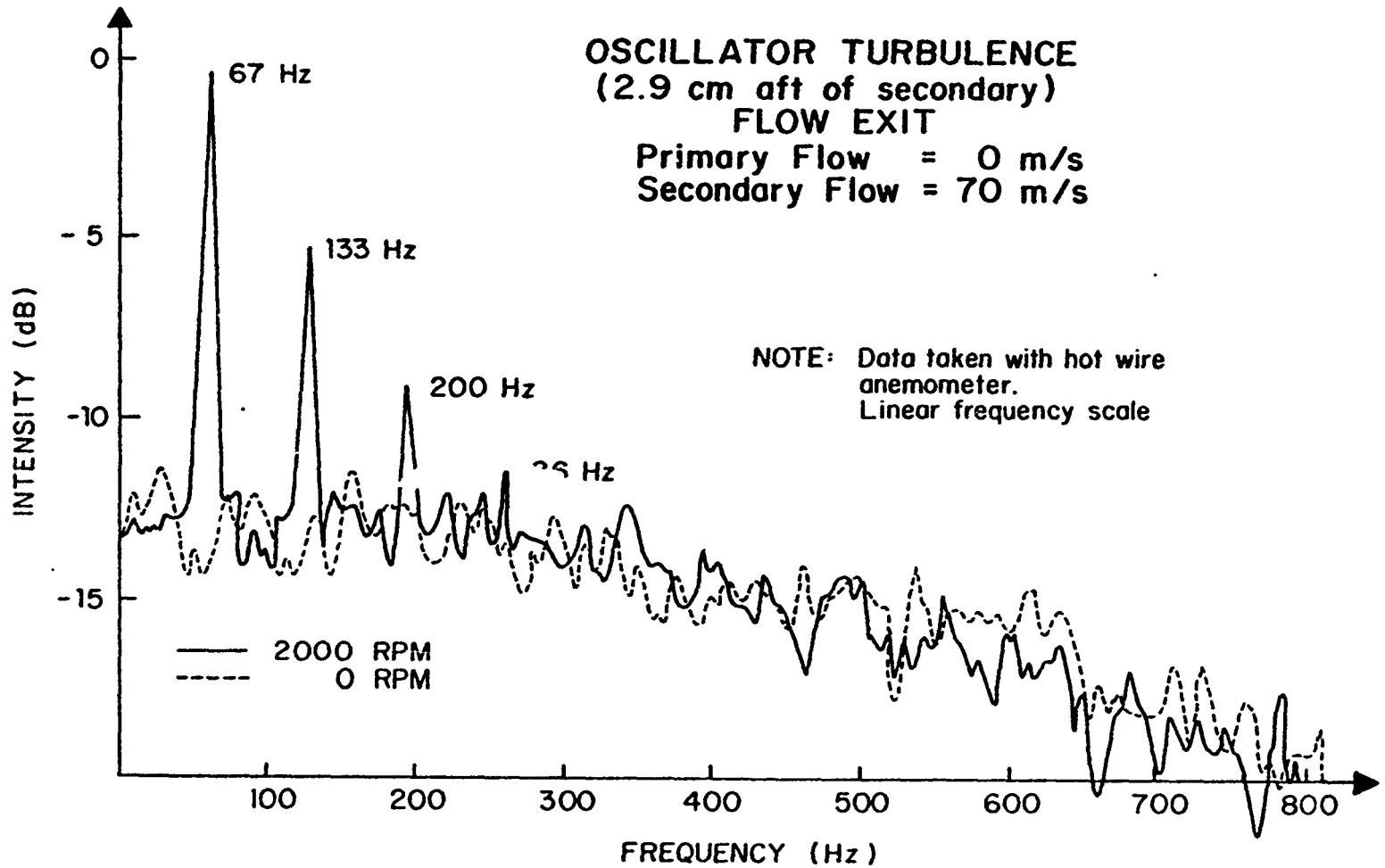

Fig. 28 Low Frequency Turbulence Spectra Showing Oscillator Overtones

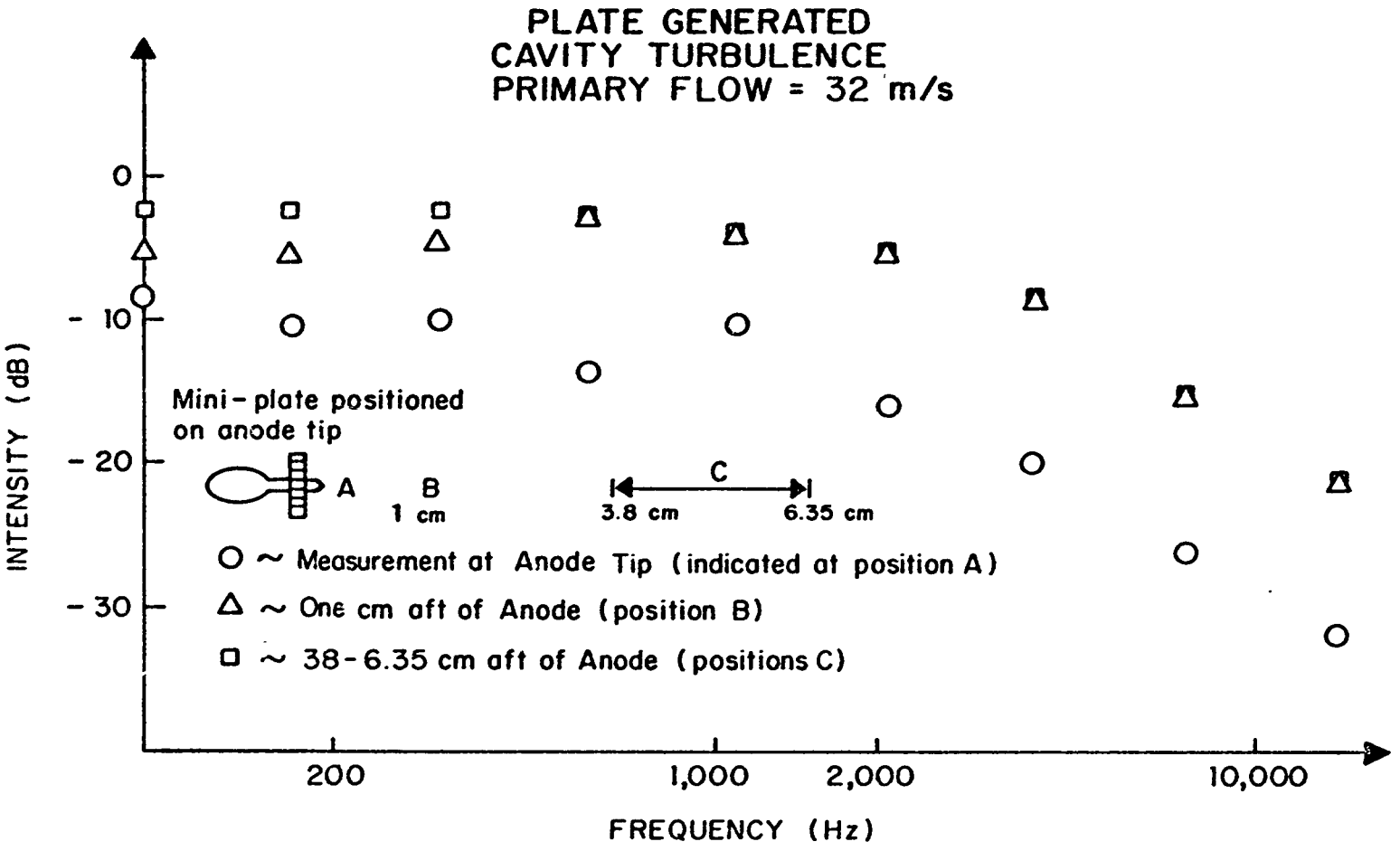

Fig. 29 Turbulence Spectra Across Gap

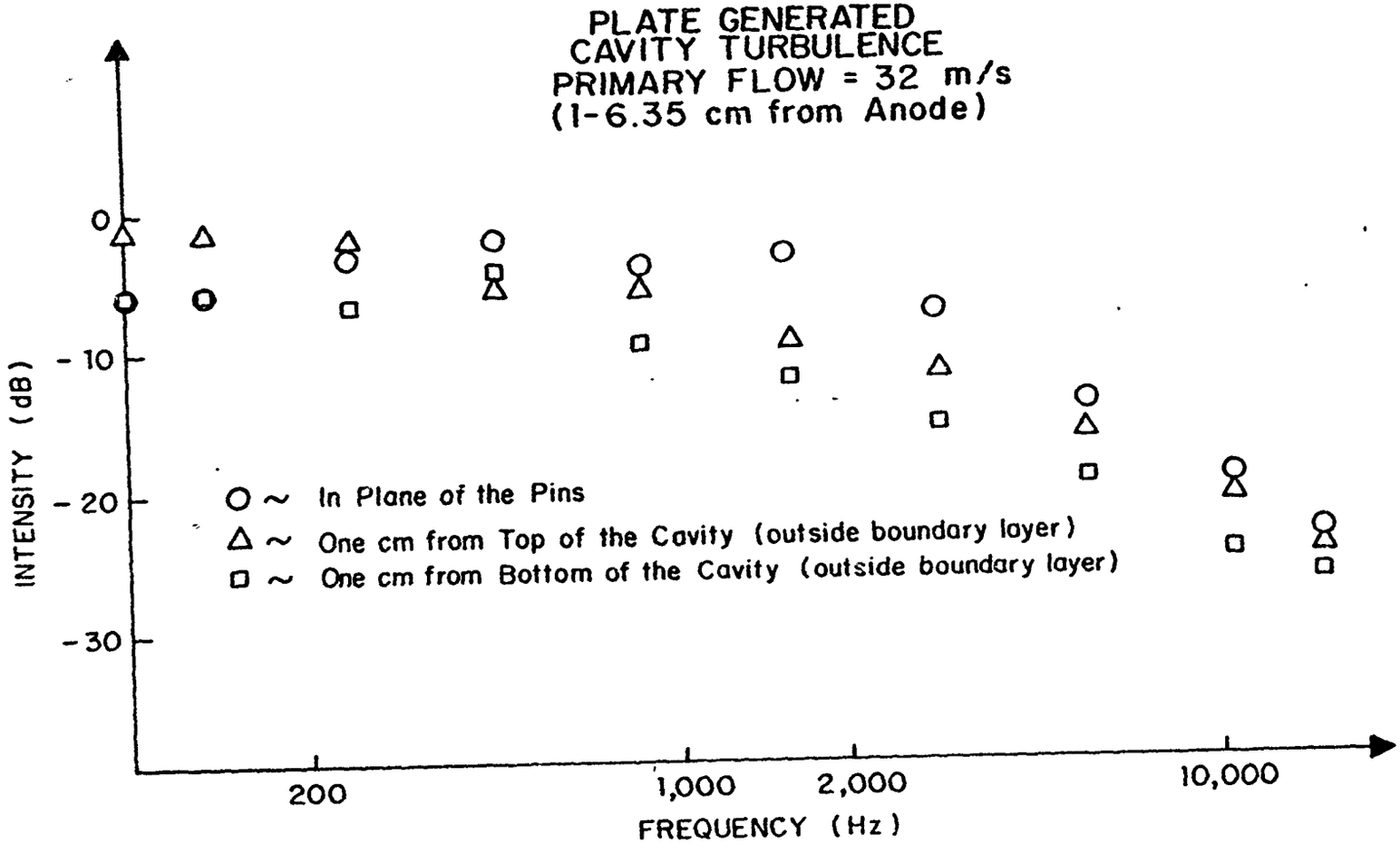

Fig. 30 Turbulence Spectra over the Cross-Section of Cavity

nozzle, Plate IX and the test cavity of Barto and Post, who employed the primary flow only. Turbulence spectra generated by the oscillator combined with the "mini-plates" are shown in Figs. 31 and 32. In Fig. 33, a comparison between the combined turbulence and the turbulence generated by the oscillator only is shown. The results of the test are discussed in Sec. V.

B. DISCHARGE PERFORMANCE TESTS

After analyzing the turbulence spectra, discharge power was investigated for various flow combinations, interelectrode gaps and RPM's that appeared interesting without the "mini-plates". As mentioned earlier, the RPM's refer to the revolution of the egg-shaped cylinder. Constant voltages below breakdown were set while the secondary flow velocity and RPM were changed. For each flow condition the voltage was increased to breakdown and the voltage and current noted (Figs. 34,35,36). Discharge power was recorded with the "mini-plates" on the anode tip at increasing primary flows, then the "mini-plates" were moved aft on the anode pins and power recorded at the same flow rates. The relative positions of the "mini-plates" are shown in Fig. 37 and the breakdown power inputs for each position is shown. In Fig. 38 and 39, breakdown current is recorded for varying secondary and primary flows at a constant RPM of 500. Finally in Fig. 40, the breakdown

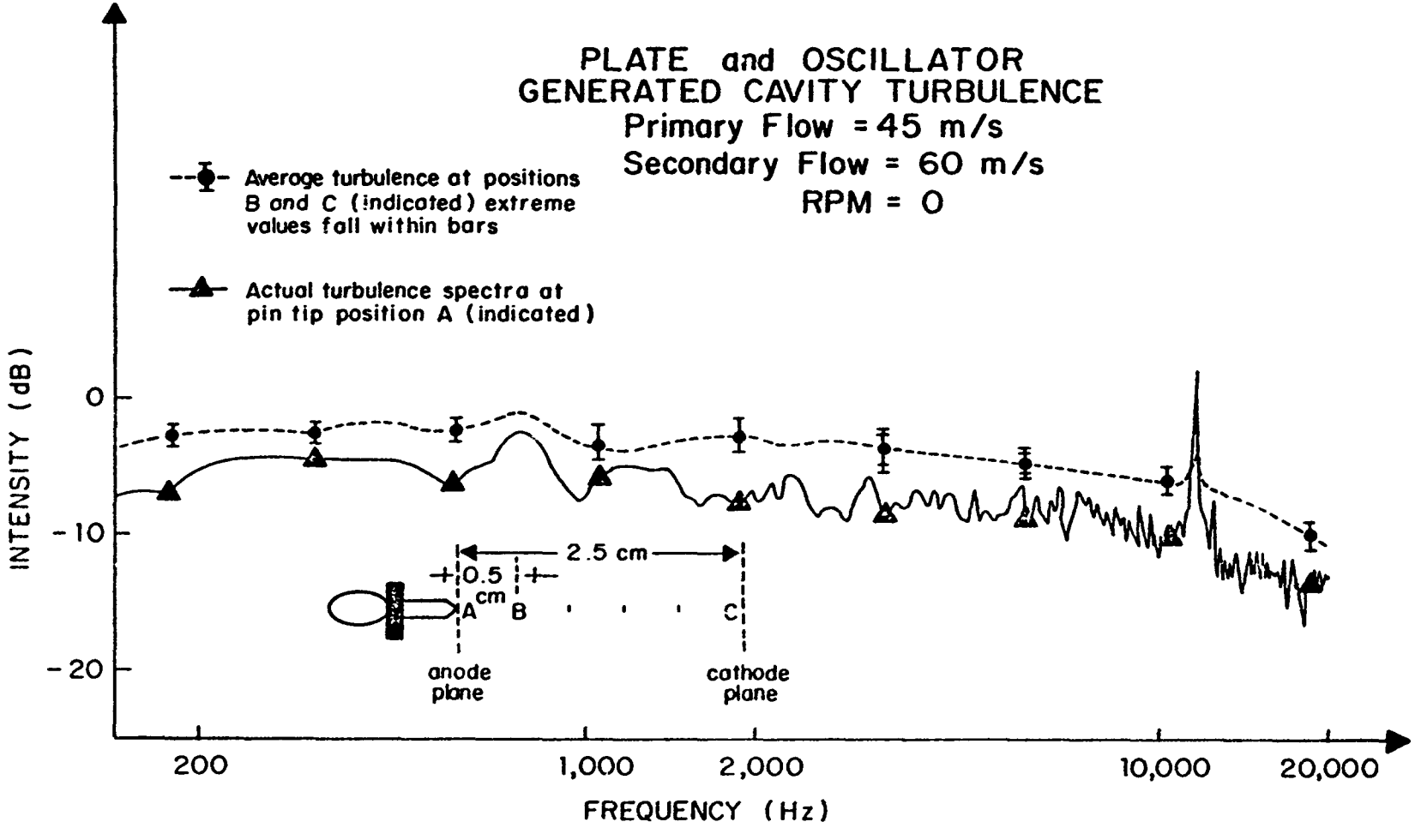

Fig. 31 Combined Generation Turbulence Spectra at Various Cavity Positions

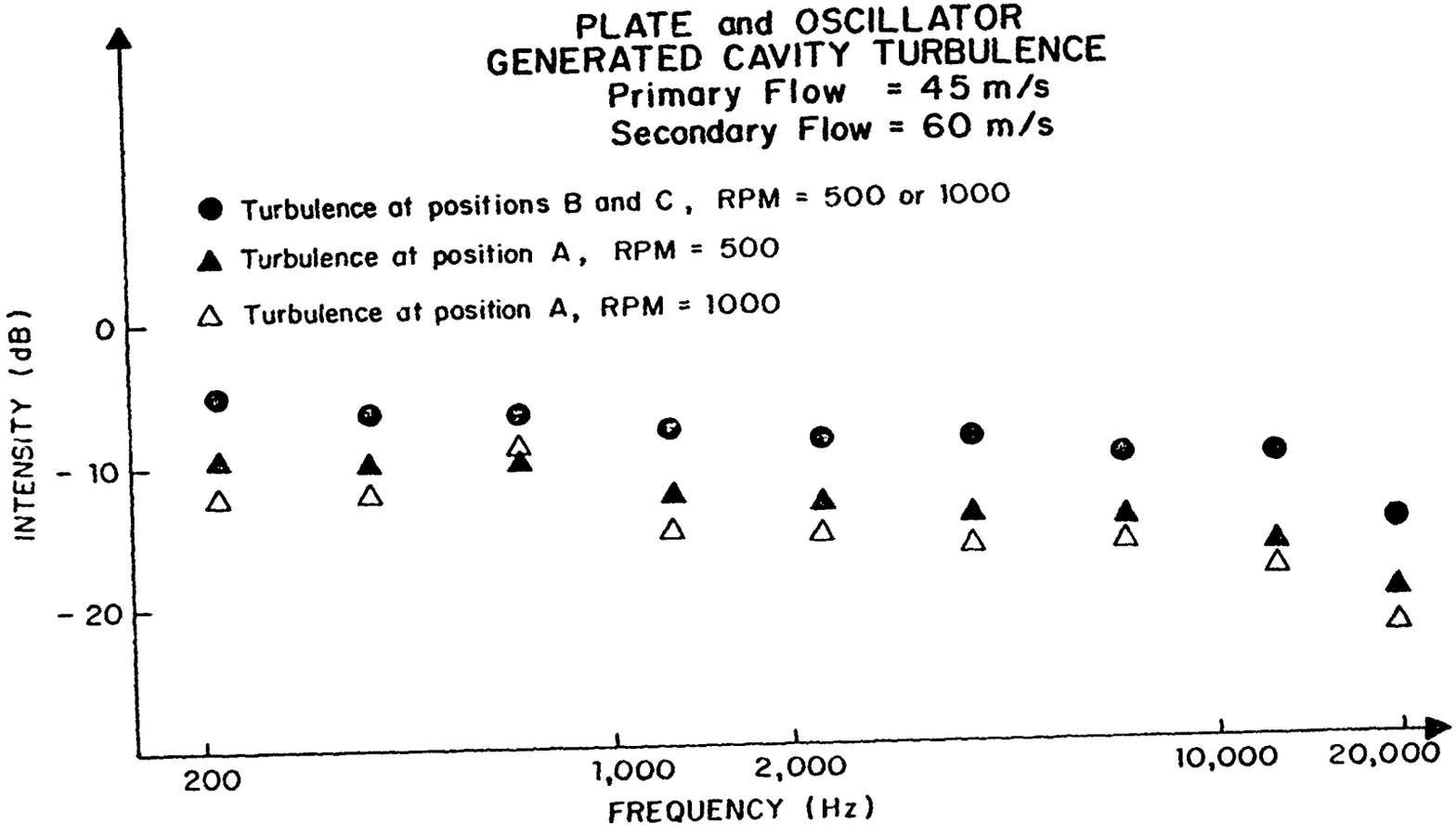

Fig. 32 Combined Generation Turbulence Spectra at Various Cavity Positions

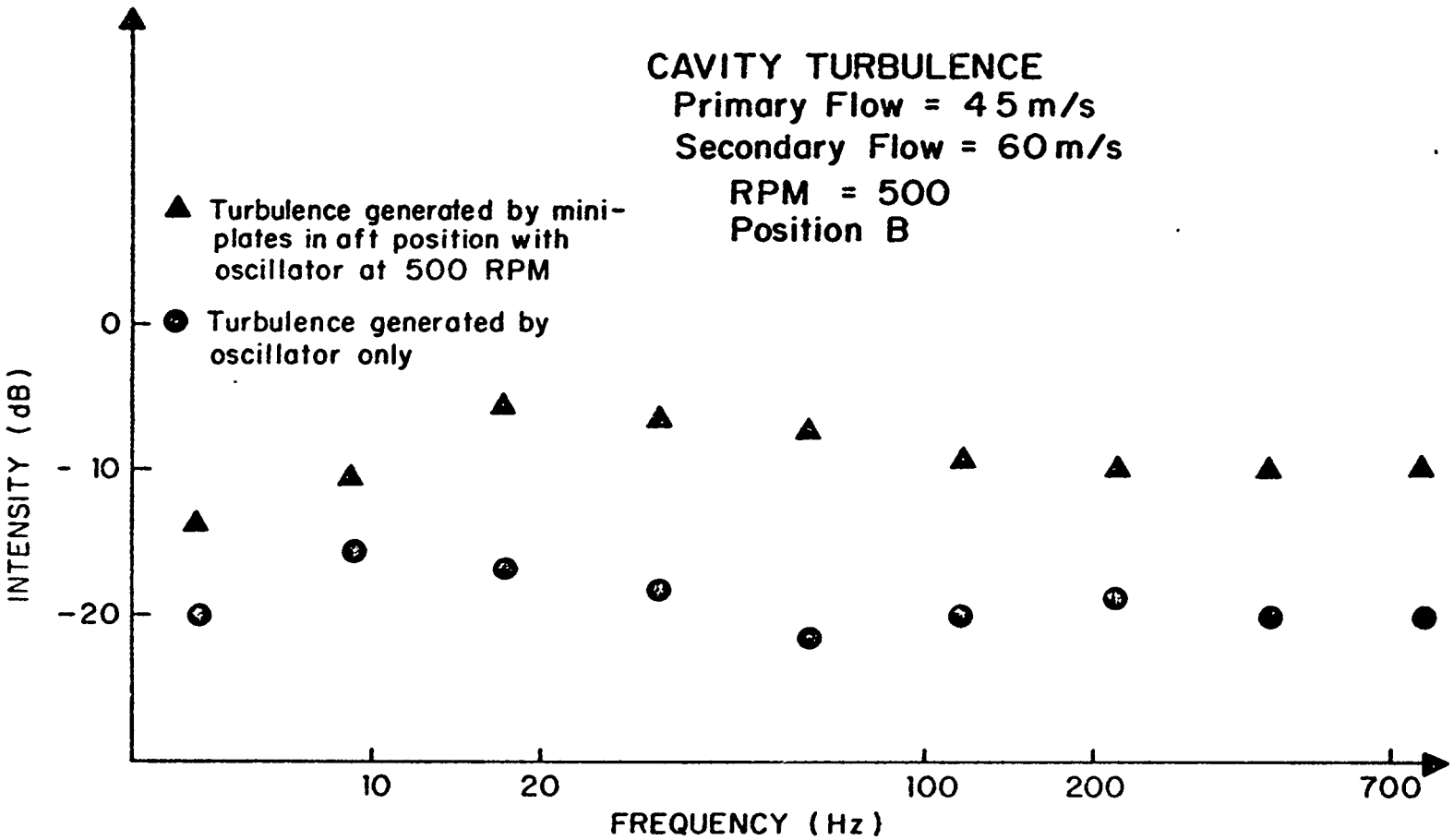

Fig. 33 Comparison of Turbulence Spectra (Combined vs. Oscillator Only)

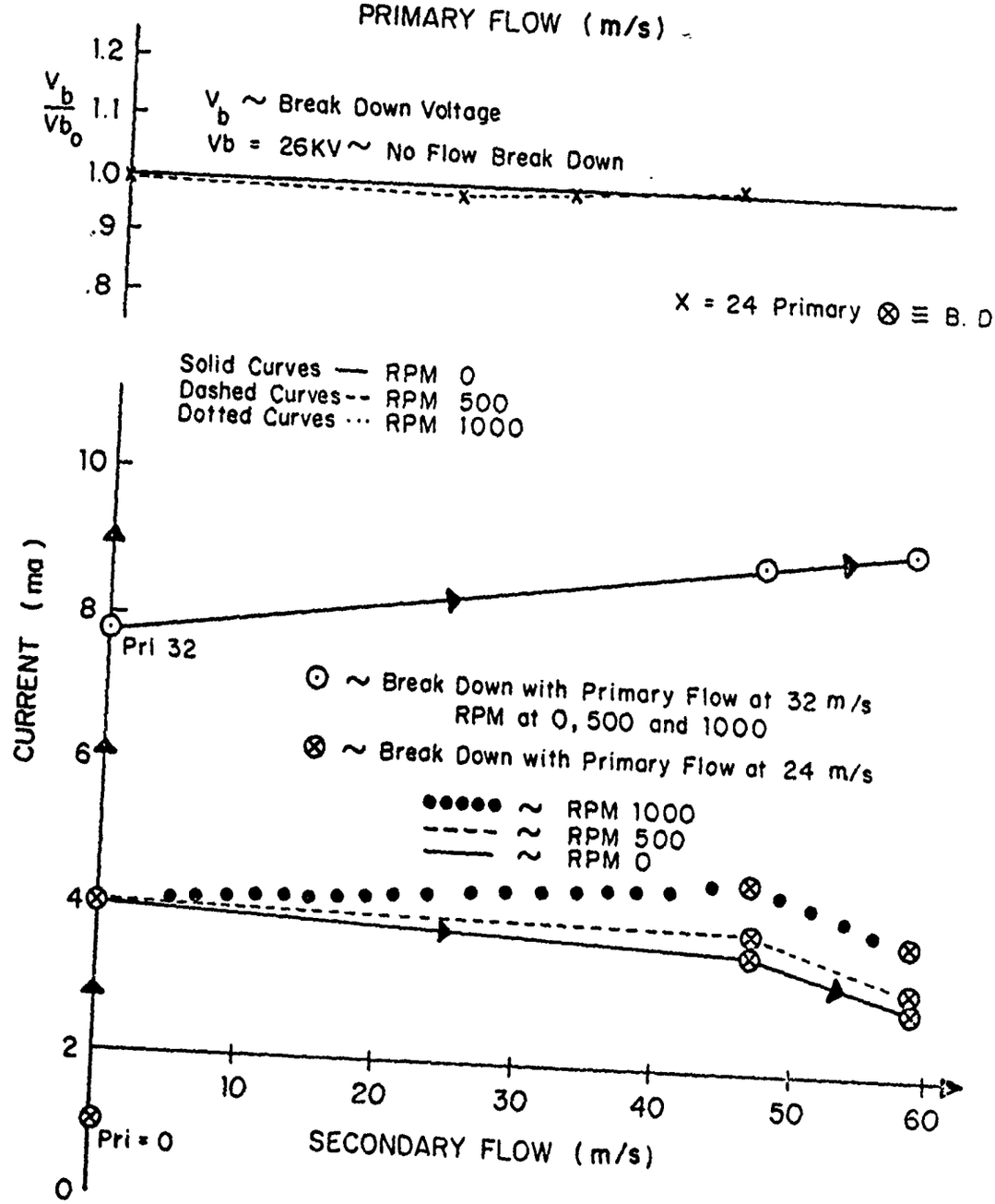

Fig. 34 Secondary Flow and Triple Slit Oscillator Effects on Break Down
(Triple Pin Row, No Grid)

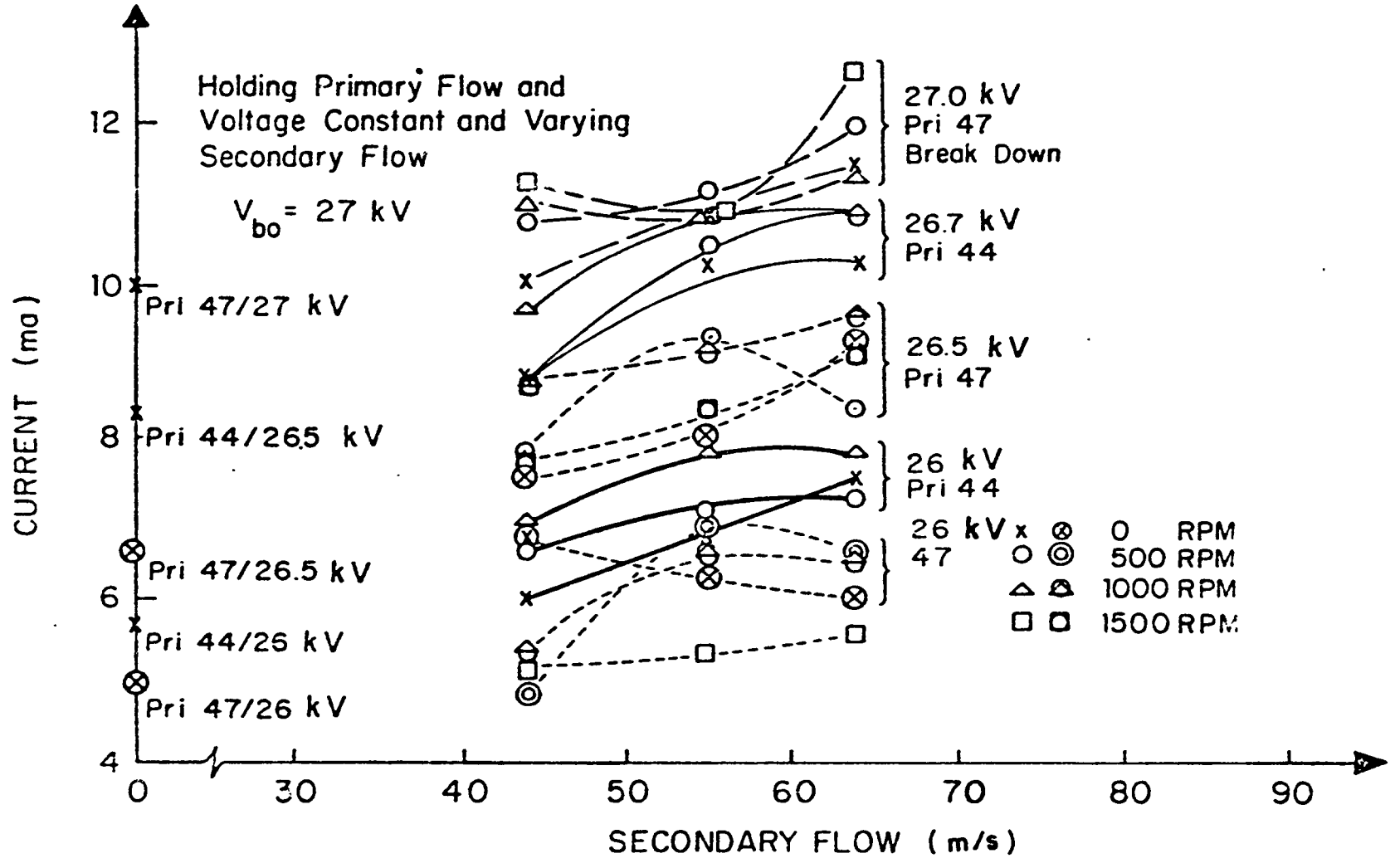

Fig. 35 Secondary Flow and Triple Slit Oscillator Effects on Current
(Triple Pin Row, No Grid)

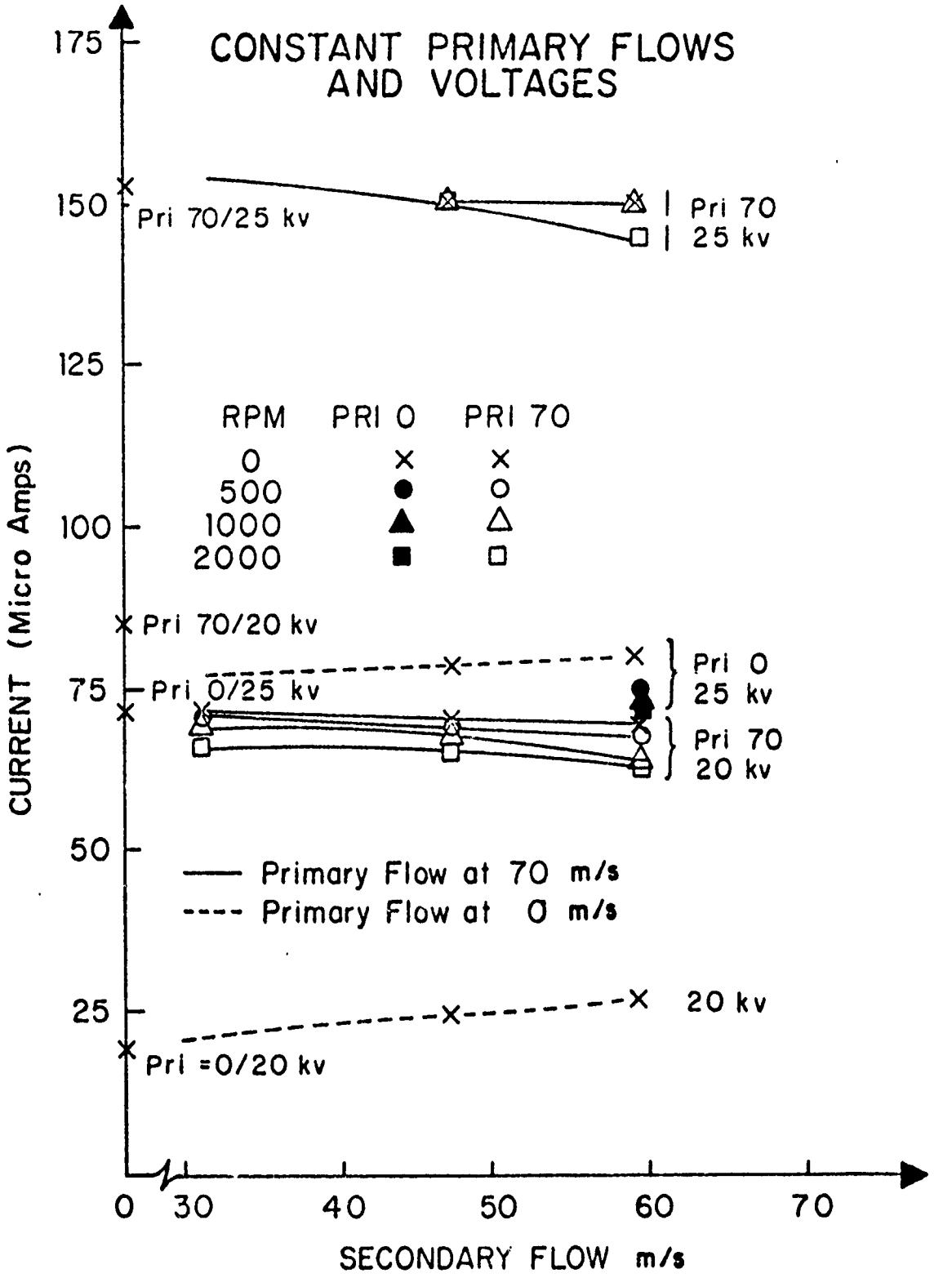

Fig. 36 Secondary Flow and Triple Slit Oscillator on Current (Triple Pin Row, No Grid)

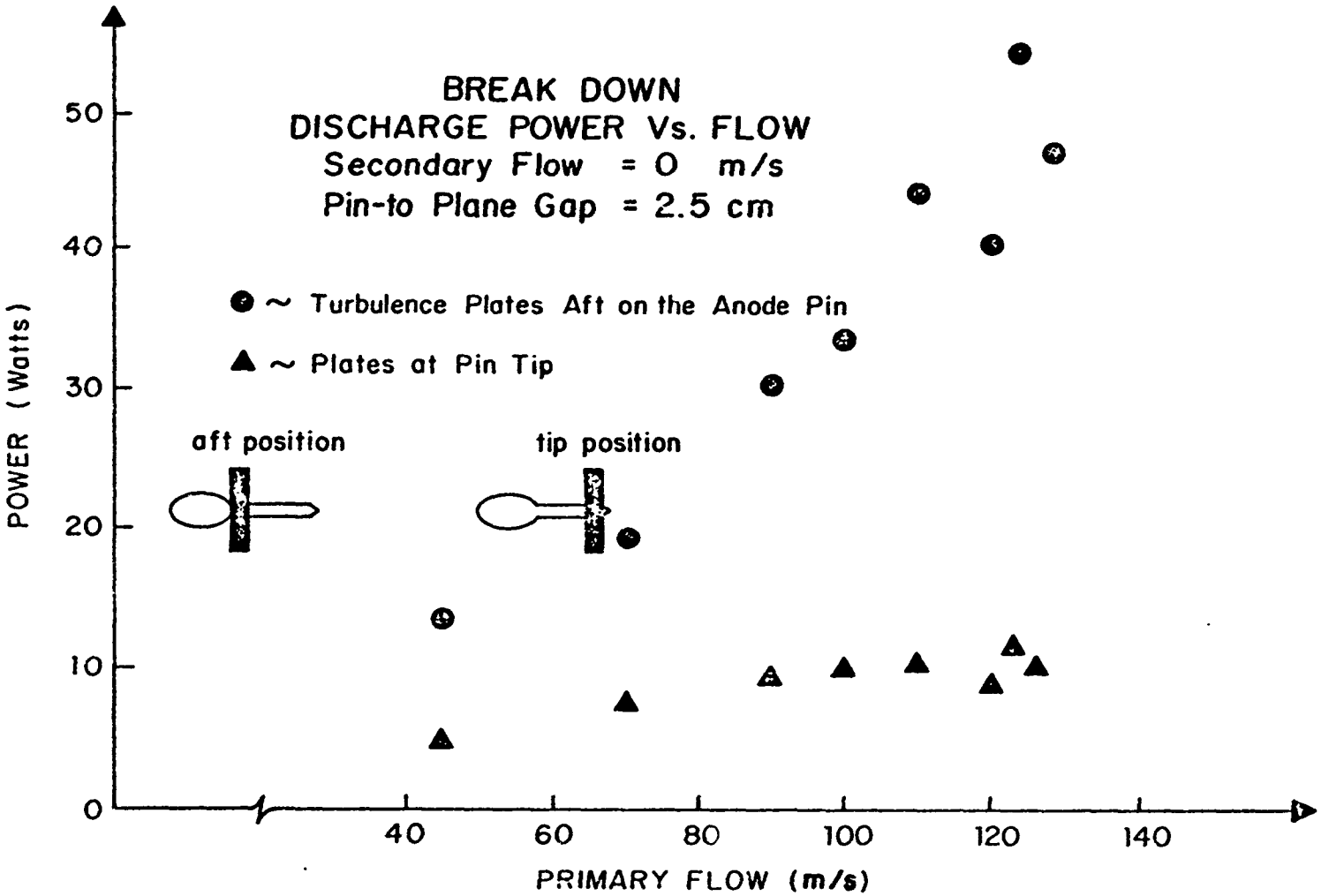

Fig. 37 Discharge Power Input as a Function of Plate Position

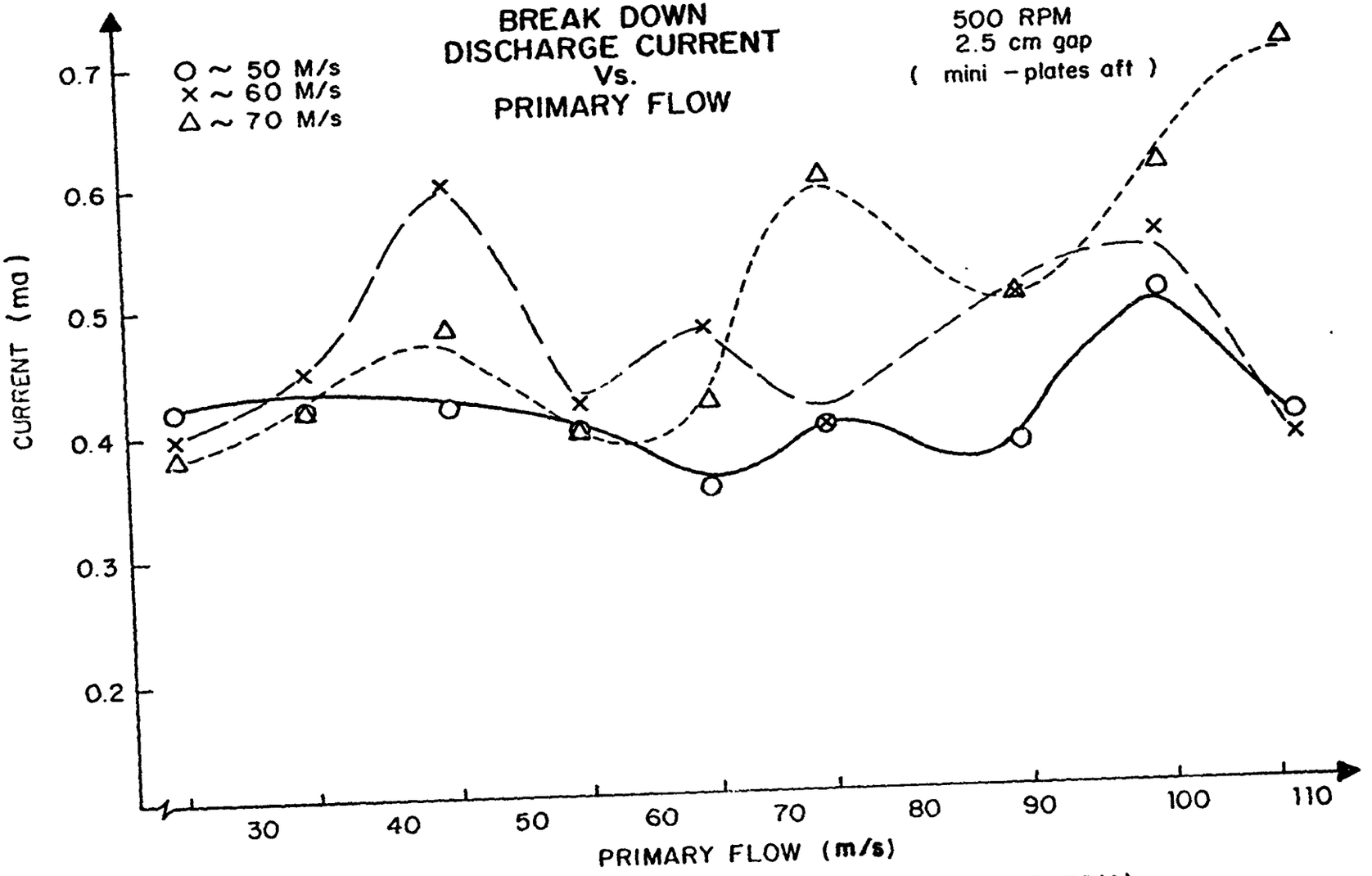

Fig. 38 Secondary Flow Effects on Current for Varying Flow (500 RPM)

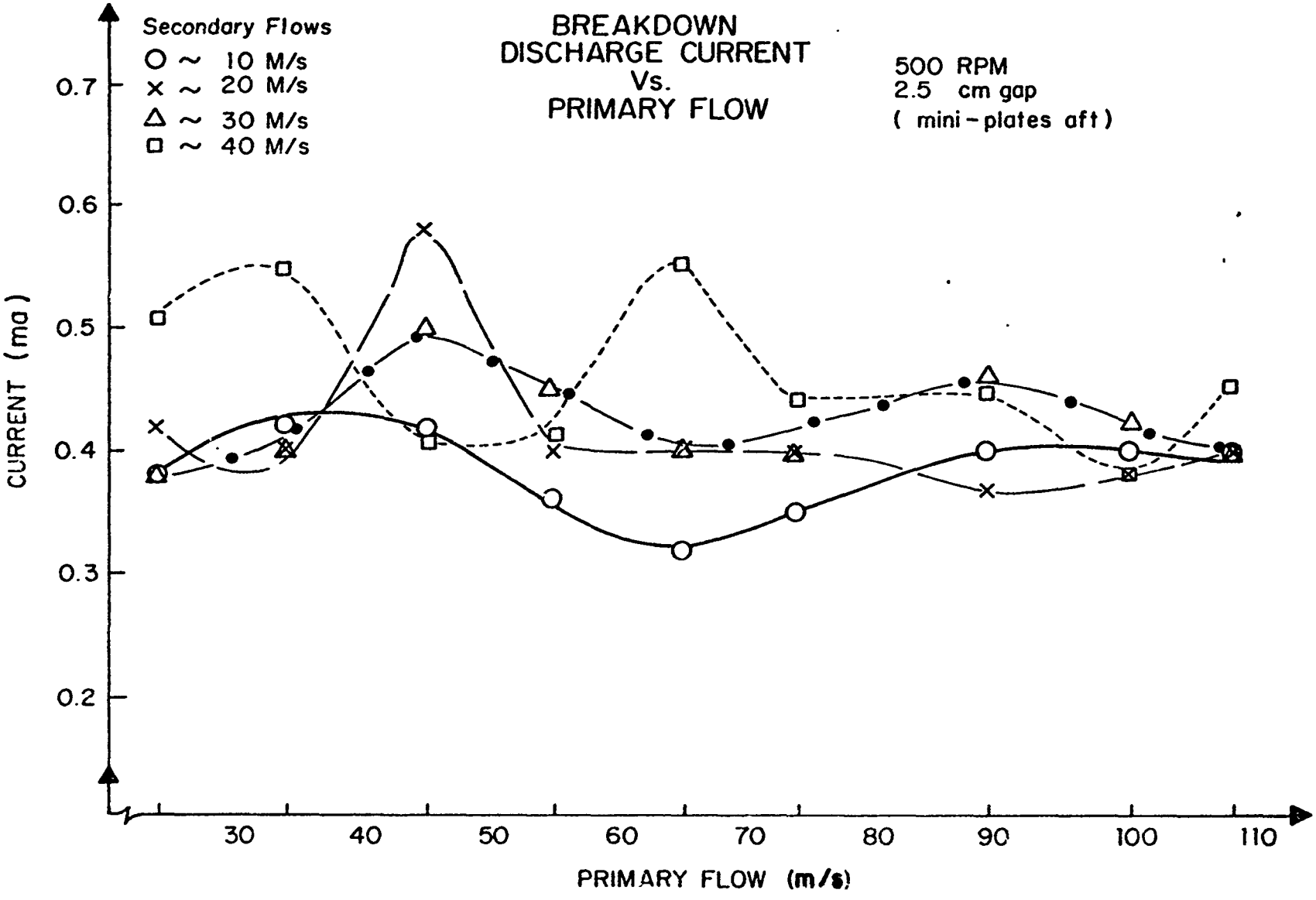

Fig. 39 Secondary Flow Effects on Current for Varying Primary Flows (500 RPM)

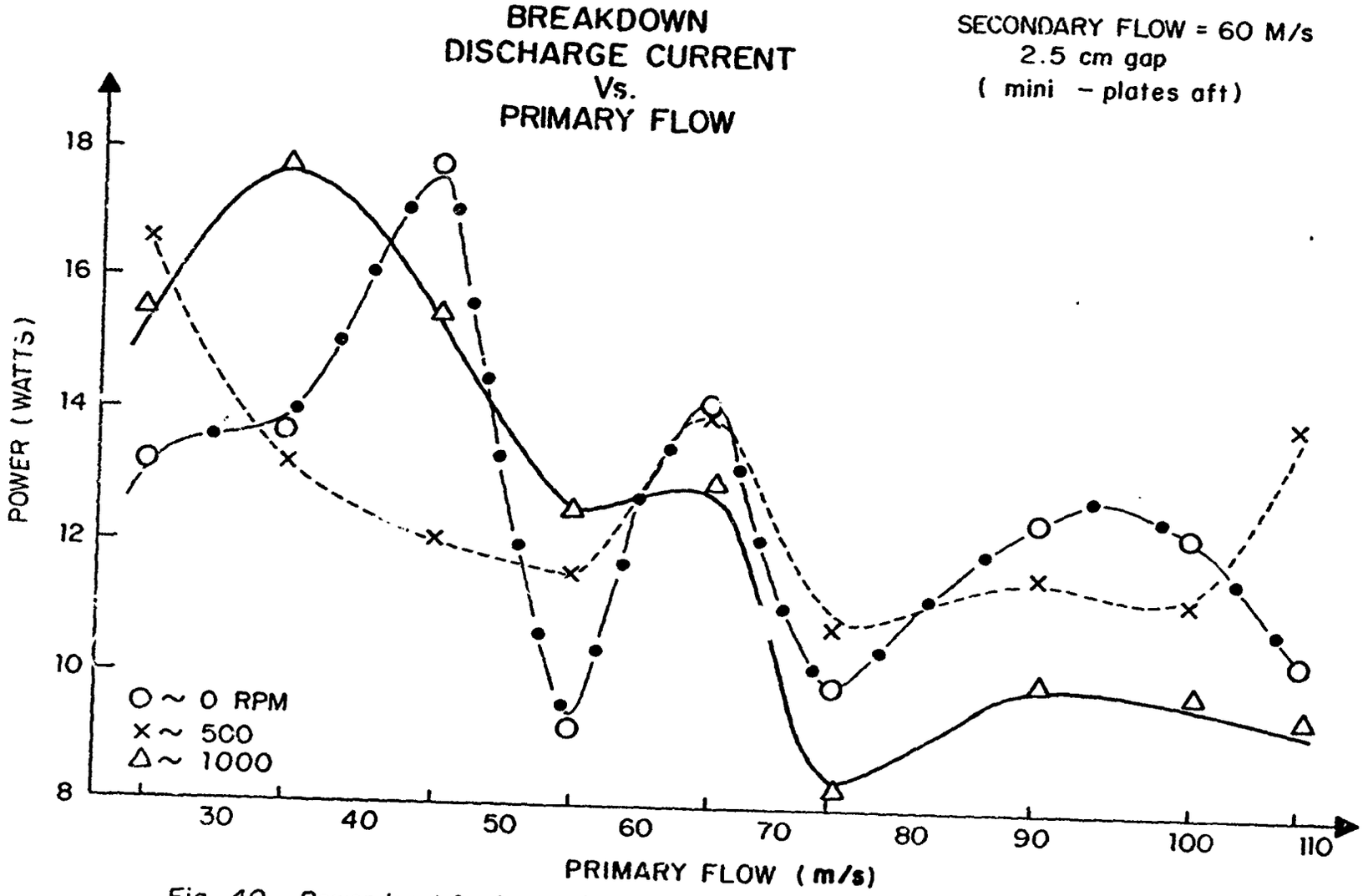

Fig. 4C Power Input for Increasing Primary Flow at Varying RPM (Constant Secondary Flow)

power inputs for a secondary flow of 60 m/s and various RPM's and primary flows are shown. These data are also discussed in Sec. V.

C. OTHER TESTS

In an effort to find the optimum turbulence frequency for this set-up, a best primary and secondary flow configuration were selected based on the data obtained and a discharge current set below breakdown while the RPM was varied from 0 to 2000. The primary flow was 45 m/s, the secondary flow was 60 m/s and the current set at 2 mA (below breakdown for all RPM). As the RPM was varied from 0 to 2000, the current stayed constant, i.e., no changes in current were apparent with oscillator RPM variation.

Velocity profiles were measured in order to ascertain how they varied along the cross section. Using a pilot-static tube, the velocity was found to be constant outside the boundary layer from side to side in the test cavity with a primary flow velocity of 90 m/s. However, moving from the bottom to the top the velocity profile retained the value of 90 m/s, dropping to 75 m/s in the middle and reaching a maximum of 105 m/s in the top half of the test cavity. This profile variation is believed to be due to the blockage arising from the secondary flow channel.

V. DISCUSSION OF RESULTS

The breakdown discharge current and power are seen to exhibit only small changes as the turbulence was varied using the oscillator flow only. In Fig. 34, with the primary flow at 24 m/s, the best breakdown performance was achieved with the secondary flow at 47 m/s and RPM at 1000. The current of 4.5 mA was less than a 1 mA improvement over the effects of convection only in which the current was already 4 mA. Note also that the breakdown voltage was virtually constant with various flows. The current was actually lower for a secondary flow of 60 m/s. When the primary flow was increased to 32 m/s, the current was almost 8 mA and as secondary flow was increased to 90 m/s the breakdown current increased to about 9 mA. The oscillator had no effect on the power with the primary flow at 32 m/s. These data were taken with the triple pin row.

In Fig. 35, higher primary flows and secondary flows were investigated with the oscillator only on the triple pin row anode. Again, the breakdown voltage was constant at 27 kV at the secondary flow and RPM was varied. These data were taken on the same day and the higher primary flow rate of 47 m/s (versus 45 m/s) consistently resulted in less current as the secondary flow and RPM were varied. For both

primary flows, the currents increased as the secondary flow increased from 47 m/s to 60 m/s. This increase in current could likely be attributed to the probable smoothing of the velocity profile in the middle of the cavity, making the effects of convection homogeneous through out the cavity. For the RPM setting of 500 and 1000 at a secondary flow of 60 m/s, the currents were one to two milliamps higher than the zero RPM conditions and almost three milliamps higher than the primary flow only currents. The oscillator had less pronounced effects on the breakdown currents.

In Fig. 36, the primary flow was increased to 70 m/s and the current did not change appreciably with increasing secondary flows and various RPM settings. This total inelasticity of current to RPM may indicate that the turbulence is being blown out of the cavity so fast that the conditions in the cavity are essentially steady state. For example, consider a flow velocity of 10^4 cm/s and a frequency of 2000 Hz, then the time to cycle from a high pressure to a low pressure and back to a high pressure is $\tau = 1/f = 0.5 \times 10^{-3}$ sec. Therefore, any point in the cavity is at enhanced or reduced pressure for $\tau/2$ seconds at a time. The distance covered by a gas particle in this time due to the flow is the half-wavelength

$$\lambda/2 = (\tau/2)\ V = (0.5 \times 10^{-3}/2)\ 10^4 = 2.5 \text{ cm} \qquad (21)$$

In other words, a test cavity gap of 2.5 cm is under the same pressure conditions (either high or low) at the same time. Therefore, breakdown should occur or current conditions will be determined by the weakest conditions due to oscillations of a single frequency. (Recall that turbulence intensity and frequency causes density fluctuations. Examine Eq. 17 again and see how the pressure fluctuations affect the ionization.) The velocity of the fully developed flow and the length of the cavity then become important parameters in optimizing turbulence stabilization effects on the electric discharge. For the flow velocity and cavity gap in the example above, frequencies lower than 2000 Hz would not be useful because they are too slow to affect the discharge medium in the distance of the cavity gap. Therefore, an important design criterion is

$$2L_c/\lambda \leq 1 \tag{22}$$

where L_c is the cavity length.

It is also apparent that the turbulence is blown out of the cavity too fast by examining Figs. 38, 39 and 40. In Fig. 38, the highest currents occur at primary flows of 50, 60 and 70 m/s as opposed to the lower secondary flows of 10, 20, 30 and 40 m/s of Fig. 38. The observed increase in power at the higher primary flows in Fig. 39 is most likely

due the overall increase in mass flow rates (due to higher secondary flow also) and the increasing benefits of convection not turbulence. In Fig. 38, the effects of convection are not overwhelming at the high primary flow because of the lower mass flow rate due to lower secondary flows. In both Figs. 38 and 39 peak powers are observed with the primary flow at 45 m/s. The highest peak was for a secondary flow of 60 m/s, which was investigated further and the results are shown in Fig. 40. In Fig. 40, breakdown power was recorded for varying RPM and primary flows above 25 m/s. The highest power was observed at a primary flow of 45 m/s and a secondary flow of 60 m/s; the turbulence spectra for these flow conditions are summarized in Figs. 31, 32 and 33. The curves depicted in Fig. 40 have the appearance of exponentially damped sinusoids that have been phase changed by the RPM. This influence of RPM is evident in spite of the fact that oscillator-generated turbulence spectra were observed to have lower intensities than the plate generated turbulence spectra as shown in Fig. 33.

Fig. 40 can be separated into two regions with the division at a primary flow of 65 m/s. At this primary flow, the velocity profile is most uniform and the breakdown power is almost the same for the three different RPM settings. This power can in fact be said to be independent of RPM entirely. In the region to the right of 65 m/s (higher primary flows), the oscillator has little

effect, the phase shift is absent and the curves fall relatively close to one another for a given primary flow. Furthermore, in this region of higher primary flows, the input breakdown power is lower due to the reduced effect of turbulence. The turbulence of the secondary flow has been buried in the increasing mass flow rate of the primary flow and is being "blown out" of the cavity too fast.

In the region to the left of 65 m/s, the velocity profile is more like the one shown in Fig. 16. Recall that when the mass flow rates of the primary and secondary are matched, the best mixing is obtained. For our set-up, the primary flow of 35 m/s would provide the best mixing for a secondary flow of 60 m/s. As stated earlier, the power inputs are phase shifted sinusoids with various RPM. Therefore, the low frequency RPM do appear to be having an effect on the discharge instabilities. Exactly which frequencies are intensified cannot be directly established by examining the turbulence data because of the similarities of the measured results in Figs. 31 and 32. These spectra were obtained by using the probe which may be averaging the intensities to see the enchancement of discrete turbulence frequencies as shown in Fig. 28 which was taken with the hot-wire anemometer.

The question of which low frequencies may be causing the phase shifting for zero RPM is even more complex. The low frequency spectra for the mini-plates has been shown to be

relatively intense for a primary flow of 32 m/s in Figs. 29 and 30 as well as a primary flow of 45 m/s and secondary flow of 60 m/s in Fig. 31. But these spectra were again taken with the pressure transducer and, as expected, no one frequency is seen to be predominant in Figs. 29, 30 and 31. However, for the flow conditions of Fig. 31 at zero RPM which fall in the lower region of Fig. 40 (best ejector mixing), the Kelvin-Helmholtz (or hose) type of instability may manifest itself. This hydromechanical instability in the viscous liquid sheet from the secondary flow ejector produces a waviness like that from a flapping jet (antisymmetric instability modes). Weihs [Ref. 42] asserts that classically the wave increases with time and is a function of fluid viscosity, surface tension and sheet velocity. He further states that there is no single wave that has a maximum growth rate, but that the wavenumber for maximum instability increases with the distance from the nozzle orifice. If the inviscid flow assumption is made, a single wave of maximum instability can be theoretically obtained from

$$k = \rho V^2 / 2\tau \qquad (23)$$

where k is the wave number, ρ is the density of the fluid, V is the velocity and τ is the time and position varying shear stress. Weihs concludes that more work needs to be

completed before a model can be successfully developed to predict the wave motion in cases of practical interest.

(The author had a habit of feeling the various flows with his hand and noticed that the flows without the oscillator operating were smooth while the vibrations could be felt in the flows with various RPM's set. On one puzzling occasion, a vibration was noticed when the RPM was zero. As an afterthought, the vibrations in the flow with zero RPM may have been the Kelvin-Helmholtz instabilities affecting a low frequency oscillation similar to that of the pulsed jet.)

Turbulence spectra for the oscillator generated turbulence are summarized in Figs. 24-28. In Fig. 24, the addition of 1000 RPM to the secondary flow is seen to shift the spectrum to the right and slightly increase the intensity. The turbulence for these secondary flows of 40 and 56 m/s is seen to develop uniformly across the cavity. Figure 25 shows the intensity of the turbulence generated by primary flow of 74 m/s and this intensity varied as much as 10 dB across the cavity. At a primary flow of 89 m/s, the intensity is again more uniform and about 5 dB more intense as shown in Fig. 26. Figure 27 shows that turbulence spectra for improperly matched flows are virtually inelastic to RPM changes, except for some enhancement below 200 Hz by a primary flow of 89 m/s, secondary flow of 55 m/s and 1000 RPM. Figure 28 displays how the oscillator can excite one

frequency and its harmonic; these data were taken with the hot wire.

The turbulence generated by the mini-plates is shown in Figs. 29, 30 and 31. Figure 30 indicates that the turbulence fills the cavity well, but turbulence is most intense in the plane of the pins (where the turbulence is most needed). The turbulence spectrum in Fig. 29 was taken in various positions in the cavity in the plane of the pins with the mini-plates close to the anode tip. For the same primary flow, the turbulence spectra were identical to the one for Plate IX (Fig. 12) which was used by Post and Barto to achieve their best power input. The only difference beween those spectra was at the position directly behind the anode. Plate IX had spectra of equal intensity at all three positions: directly behind the anode, one centimeter aft of the anode in the test cavity and back to 6.5 cm aft of the anode; whereas, the intensity of the turbulence spectra is seen to be approximately 10 dB lower at all frequencies when measured at the anode tip. The turbulence spectrum with the mini-plate moved aft on the anode, as shown in Fig. 30, was seen to increase the relative turbulence intensity at the anode tip. The spectra at the anode are approximately 5 dB lower when compared to locations farther back in the cavity. (The spike in the intensity at 12,000 Hz, seen in Fig. 31, is thought to result from some "whistling" in the valving of the primary flow.)

Increasing the turbulence intensity at the anode enhances the turbulence interaction with the positive space charge. The increase in power input resulting from moving the mini-plate away from the anode tip is shown in Fig. 37 by comparison. The power level measured in this configuration is not as high as that achieved by Post and Barto with Plate IX, but a direct comparison is difficult for two reasons. First, the Barto-Post anode had three pin rows, hence three times the power input would be expected. Second, there is uncertainty due to variation in atmospheric conditions and their effects on breakdown current. (An error analysis is presented in Ref. 30). Notice that the turbulence in Fig. 31 still does not have as much intensity at the anode even with the mini-plate moved away from the tip. Plate IX still has better turbulence performance at the anode than the mini-plates at the expense of considerably more flow energy input.

VI. CONCLUSIONS

High intensity, low frequency turbulence stabilizes the electric discharge as shown by the combined turbulence generation power input of Figs. 38-40. However, higher frequency turbulence also enhances power inputs as shown in Fig. 37; with the faster flow rates, the low frequency turbulence is being blown out of the cavity, but the power input is greater for the increased turbulence intensity at the anode tip. High intensity turbulence in the positive space charge region at the anode tip appears to be critical for discharge stability.

Control of the low frequency turbulence spectrum is possible through the pulsed-jet ejector principle. Both discrete peaks of frequency and intensity can be easily varied. Two factors detracted from the effectiveness of this turbulence generation scheme on the discharge stability problem. First, at certain combinations of interelectrode gaps and flow velocities, the low frequency turbulence may affect the pressure fluctuations too slowly to stabilize the discharge and is effectively blown out of the cavity. Second, the discharge stabilization problem is a three-dimensional problem and the turbulence generated by the slit

in the nozzle can be essentially two dimensional, i.e., this turbulence may be too uniform across the cavity width.

Turbulence generated by the mini-plates is not discrete, but has impressive discharge stabilization effects. The location of the turbulence peak can be controlled by moving the mini-plates along the anode length. Although there are velocity and turbulence deformities at the anode tip, these may be overcome by a combination of redesigning the anode tip or the mini-plate. Some suggestions are made in Sec. V.I. The mini-plate turbulence generators do not substantially increase the back pressures in the primary flow and for this reason are much more efficient than Plate IX which caused a fifty percent increase in back pressures for the same flow velocity. However, the velocity defect due to the mini-plates at the anode tips tends to be quite severe.

Scatter in the current voltage data is evident in this work and may be attributed to changes in humidity of the flows and to statistical variations of activity at the anode pins.

VII. RECOMMENDATIONS

Future studies may benefit by implementing the following recommendations.

1. Better instrumentation would permit more reliable results to be obtained more easily; for example, data had to be calibrated for rather gross fluctuations in ammeter readings. The spectrum analyzer could not be averaged for more than four seconds due to an internal malfunction (which we were unable to correct).

2. The control over the rotating egg-shaped cylinder was also crude. Low frequency oscillations (below 750 RPM) were difficult to obtain. The readout for oscillator RPM fluctuates widely, which makes setting RPM's to tolerances of $\pm$100 RPM difficult. In addition, the fine voltage control on the power supply was too gross for the low RPM's. A very small movement in the control in the low range produced as much as a 1000 RPM change. A system should be developed where an RPM setting can be obtained within $\pm$20 RPM (within one minute). A power supply with a finer vernier voltage control and a more accurate RPM readout would be helpful.

3. Obtain more data with the turbulence generating mini-plates working in conjunction with the oscillator at an optimum primary flow for button placement. Determine if the low frequency oscillations of the jet pulsing are affecting

the flow at the anode tip. Consider, especially, the conditions where the primary and secondary mass flow rates are matched for the best mixing. These flow rates should be kept low enough so that the turbulence is not blown out of the cavity. An alternative to lower flow rates would be to investigate much longer interelectrode cavity gaps.

4. As a modification to recommendation three above, investigate the possibility of running two oscillating flows: one to enhance the large scale turbulence and the other to enhance the high frequency turbulence. In the interim, the efficiency of the present oscillator could be improved by having the slit in the nozzle re-engineered to incorporate seven holes across the nozzle exit. This may enhance the three dimensional mixing.

5. Lower blockage pressures could be obtained by acoustical generation of the required turbulence. This lower back pressure is obtained by mounting the speakers on the sides of the cavity. Acoustically generated turbulence may be more efficient because of the lower back pressures and hence the possibility of a lower work input. Acoustic turbulence spectra can be easily varied to enhance certain ranges of frequencies, especially in the lower ranges. Only relatively low intensities have been attainable acoustically in the higher frequencies of the turbulence spectrum [Ref. 24].

6. Re-engineer the anode tips making them longer so the mini-plates have more adjustment distance.

7. Re-design the mini-plates to permit more fluid to pass close to the surface of the anode sooner to break-up the boundary layers and have more turbulence at the anode tip. Making the tip of the anode thinner may assist this process of overcoming the flow velocity and turbulence deficiencies at the anode tip.

8. Use the hot-wire anemometer or the laser velocimeter to investigate flows where discrete frequencies are to be intensified. Compare these measurements with measurements taken by the pressure transducer to calibrate its response.

LIST OF REFERENCES

1. Garrett, C. G. B., Gas Lasers, New York: McGraw-Hill, 1967.

2. Sinclair, D. C. and Bell, W. C., Gas Laser Technology, New York: Holt, Rinehart, and Winston, Inc., 1969.

3. Patel, C. K. N., "Vibration Energy Transfer - An Efficient Means of Selective Excitation in Molecules", Physics of Quantum Electronics, Kelle, Lax and Tannenwald, eds., New York: McGraw-Hill, 1966.

4. Fuhs, A. C., "High Energy Laser System Design", notes from a course in the aeronautical engineering department of the Naval Postgraduate School, Monterey, CA, September 1979.

5. Anderson, J. D., Gas Dynamic Lasers: An Introduction, New York: Academic Press, 1976.

6. Smith, K. and Thompson, R. M., Computer Modeling of Gas Lasers, New York: Plenum Press, 1978.

7. Oshea, D. C., Introduction to Lasers and Their Applications, Reading, MA: Addison Wesley, Publishers, 1977.

8. Fowler, M. C., "Influence of Plasma Kinetic Processes on Electrically Excited CO_2 Laser Performance", Journal of Applied Phycis, 43 (August 1972): pp. 3480-3487.

9. Limbeck, J. W. and Lucas, J., "Computation and Measurement of the Fluorescent Infrared Radiation from Glow Discharges in CO_2-N_2-H_e Gas Mixtures", Solid State and Electron Devices, 2 (September 1978): pp. 155-160.

10. Cobine, J. D., Gaseous Conductors, New York: McGraw-Hill, 1941.

11. Biblarz, O., Barto, J L., and Post, H. A., "Gas Dynamic Effects on Diffuse Electrical Discharges in Air", Israel Journal of Technology, 15 (1977): pp. 59-69.

12. Deutsch, T. F., Horrigan, F. A., and Todko, R. I., Applied Physics Letters, 25 (1969): pp. 118-127.

13. Demaria, A. J., "Survey of Electric Discharge CO_2 Lasers," Proceedings of IEEE, 61 (1973): pp. 731-745.

14. Lancashire, R. B., et al., "The NASA High-Power Carbon Dioxide Laser", Optical Engineering, 16 (October 1977): pp. 505-512.

15. Jones, C. R., "Optically Pumped Mid-IR Lasers", Laser Focus, 14 (August 1978): pp. 68-74.

16. Balykin, V. I., et al., JETP Lett, 19 (1974): p. 256

17. Nelson, R. E., "Electric Discharge Stablization by Highly Turbulent Flow," M.S. Thesis, Naval Postgrazduate School, June 1973.

18. Barto, J. L., "Gasdynamic Electric discharge in Air," M.S. Thesis, Naval Postgraduate School, September 1976.

19. Meek, J. M. and Craggs, J. D., Electrical Breakdown of Gases, London: Oxford, 1953.

20. Naser, E., Fundamentals of Gaseous Ionization and Plasma Electronics, New York: Wiley, 1971.

21. Viets, H., Thrust Augmenting Ejectors. Wright-Patterson AFB, Ohio: Aerospace Research Laboratories, June 1975.

22. Johnson, W. S. and Yang, T., A Mathematical Model for the Prediction of the Induced Flow in a Pulsejet Ejector with Experimental Verification. ASME paper WA/FE-33, 1968.

23. Hill, W. G. Jr., and Greene, P. R., Self Existed Superturbulence: The Whistler Nozzle. Grumman Aircraft Corp. Research Department Report RE-488, October 1974.

24. Bevilaqua, P. M., and Lykoudis, P. S., "Entrainment and the Large Eddy Structure," AIAA Paper No. 75-115, 1975.

25. Biblaz, O. and Fuhs, A. E., "Laser Cavity Density Changes with Kinetics of Energy Release," American Institute of Aeromautics and Astronautics Journal, 12 (August 1974): pp. 1083-1089.

26. Fuhs, A. E., and Biblarz, O., "Laser Aerodynamics," Naval Research Review, 29 (1976): pp. 11-13.

27. Wiegand, W. J. and Nigham, W. L., "Influence of Fluid Dymanic Phenomenon on the Occurrence of Constriction in CW Convection Laser Discharges," Applied Physics Letter, 26 (1975): P. 554.

28. Biblarz, O. and Nelson, R. E., "Turbulence Effects on an Ambient Pressure Discharge," Journal of Appled Physics, 45 (February 1974): pp. 633-637.

29. Aunchman, L. J., "Controlled Turbulence as a Design Criterion for Electric Discharge Convection lasers," M.S. Thesis, Naval Postgraduate School, March 1974.

30. Post, H. A., "Sub-amibient Controlled Turbulence Effects on Discharge Stabilization for Laser Applications," M.S. Thesis, Naval Postgraduate School, September 1976.

31. Loeb, L. B., Electrical Coronas, Berkley, California: University of California Press, 1955.

32. Wasserstrom, E., et al., "The Interaction Between Electrical Discharges and Gas Flow," Journal of Applied Physics, 49 (January 1978): pp. 81-86.

33. Bollis, R. H., Nighan, W. L., Wiegand, W. J., Investigation of the Stability of Laser Discharges. Wright-Patterson AFB, Ohio: Plasma Physics Research Laboratories, June 1975.

34. Barto, J. L., "Fundamental Nature of Gas Dynamic Interaction in Highly Non-Uniform High Pressure Electrical Discharges," NPS 67-80-005, August 1980.

35. Schlichting, H., Boundary Layer Theory, New York: McGraw-Hill, 1960.

36. Stricker, J., "Design Considerations of a Flow System for Transient Laser Discharge Experiments," NPS 67-79-008, August 1979.

37. Bremhorst, K. and Horch, W. H., "Mean and Turbulent Velocity Measurements in the Near Field of a fully pulsed subsonic Air Jet," Symposium on Turbulent Shear Flows Pennsylvania State University, April 1977.

38. Bauman, J. L., "Development of a Control Valve to Induce an Oscillating Blowing Coefficient in a Circulation Control Rotor," M.S. Thesis, Naval Postgraduate School, December 1976.

39. Platzer, M. F., "Entrainment Characteristics of Unsteady Subsonic Jets," AIAA Journal, 16 (March 1978): pp. 282-284.

40. Endevco Model 8507 Transducer Operating Manual.

41. Private communication with Professor Oscar Biblarz.

42. Weihs, Daniel, "Stability of thin, radially moving liquid sheets," Journal of Fluid Mechanics 87 (1978): pp. 289-298.

43. Binder, G. and Didelle H., "Improvement of Ejector Thrust Augmentation by Pulsating or Flapping Jets," Second Symposium on Jet Pumps and Ejectors, Cambridge, England (March 1975) p. X53.

INITIAL DISTRIBUTION LIST

		NO. OF COPIES
1.	Defense Technical Information Center Cameron Station Alexandria, Virginia 22314	2
2.	Library Code 0142 Naval Postgraduate School Monterey, California 93940	2
3.	Office of Research Administration Code 012A Naval Postgraduate School Monterey, California 93940	2
4.	Chairman Department of Aeronautics Code 67 Naval Postgraduate School Monterey, California 93940	2
5.	Professor Oscar Biblarz Department of Aeronautics Code 67Bi Naval Postgraduate School Monterey, California 93940	3
6.	LCDR J. L. Barto Department of Weapon Systems Engineering U. S. Naval Academy Annapolis, Maryland 21402	1
7.	Professor J. P. Powers Department of Engineering Code 62Po Naval Postgraduate School Monterey, California 93940	1
8.	Chairman Department of Electrical Engineering Code 62 Naval Postgraduate School Monterey, California 93940	1

NO. OF COPIES

9. LCDR H. A. Post — 1
F-4 Weapon System Manager
NARF NORIS
San Diego, California 92136

10. LCDR S. Van Brocklin — 1
Department of Aeronautics
Code 67
Naval Postgraduate School
Monterey, California 93940

11. LT. C. Davis — 3
Department of Aeronautics
Code 67
Naval Postgraduate School
Monterey, California 93940

12. Commander — 1
Naval Air Systems Command
Department of the Navy
ATTN: Dr. H. R. Rosenwasser, Code AIR 310C
Washington, D. C. 20360

13. Mr. John A. Satkowski — 1
Office of Naval Research
Power Program, Code 473
Washington, D.C. 20360

14. Dr. William L. Nigham — 1
United Aircraft Research Laboratory
East Hartford, CT 06108

15. Dr. B. N. Srivastava — 1
AVCO Everett Research Laboratory
2385 Revere Beach Parkway
Everett, Massachusetts 02149

16. CAPT T. A. Filcoff — 1
AFWL-AREP
Kirtland AFB, New Mexico 87117

17. Dr. J. Shwartz — 1
TRW System
One Space Park
Redondo Beach, California 90278

18. Dr. Alan Garscadden — 1
AFAPL/POD
Building 450/Room D101
Wright-Patterson AFB, Ohio 45433

NO. OF COPIES

19 Dr. A. V. Phelps 1
JILA
Boulder, Colorado 80309

20. Professor A. W. Cooper 1
Department of Physics and Chemistry
Code 61
Naval Postgraduate School
Monterey, California 93940

21. Dr. R. B. Lancashire 1
NASA Lewis Research Center
Cleveland, Ohio 44135

22. Professor B. E. Cherrington 1
Gaseous Electronics Laboratory
University of Illinois
Urbana, Illinois 61801

23. Dr. J. Stricker 1
Department of Aeronautics
Technion, Haifa 32000
ISRAEL

24. Dr. Y. L. Khait 1
Department of Physics
Ben Gurion University, P.O. Box 653
Beer Sheva 84120
ISRAEL

25. Commandant (G-PTE-1/72) 2
U.S. Coast Guard Headquarters
Washington, D. C. 20593